

Reaction Dynamics in Astrochemistry: Low-Temperature Pathways to Polycyclic Aromatic Hydrocarbons in the Interstellar Medium

Ralf I. Kaiser,¹ Dorian S.N. Parker,¹ and Alexander M. Mebel²

¹Department of Chemistry, University of Hawaii at Manoa, Honolulu, Hawaii 96822; email: ralfk@hawaii.edu

²Department of Chemistry and Biochemistry, Florida International University, Miami, Florida 33199

Annu. Rev. Phys. Chem. 2015. 66:43–67

First published online as a Review in Advance on November 20, 2014

The *Annual Review of Physical Chemistry* is online at physchem.annualreviews.org

This article's doi:
10.1146/annurev-physchem-040214-121502

Copyright © 2015 by Annual Reviews.
All rights reserved

Keywords

cold molecular clouds, neutral-neutral reactions, nonequilibrium chemistry, aromaticity, resonantly stabilized free radical, ISM

Abstract

Bimolecular reactions of phenyl-type radicals with the C₄ and C₅ hydrocarbons vinylacetylene and (methyl-substituted) 1,3-butadiene have been found to synthesize polycyclic aromatic hydrocarbons (PAHs) with naphthalene and 1,4-dihydronaphthalene cores in exoergic and entrance barrierless reactions under single-collision conditions. The reaction mechanism involves the initial formation of a van der Waals complex and addition of a phenyl-type radical to the C1 position of a vinyl-type group through a submerged barrier. Investigations suggest that in the hydrocarbon reactant, the vinyl-type group must be in conjugation with a $-C\equiv CH$ or $-HC=CH_2$ group to form a resonantly stabilized free radical intermediate, which eventually isomerizes to a cyclic intermediate followed by hydrogen loss and aromatization (PAH formation). The vinylacetylene-mediated formation of PAHs might be expanded to more complex PAHs, such as anthracene and phenanthrene, in cold molecular clouds via barrierless reactions involving phenyl-type radicals, such as naphthyl, which cannot be accounted for by the classical hydrogen abstraction–acetylene addition mechanism.

1. INTRODUCTION

Ever since the first postulation of polycyclic aromatic hydrocarbons (PAHs)—organic molecules carrying fused benzene rings—together with their (partially) (de)hydrogenated, ionized, protonated, and substituted counterparts as the missing link between small carbon clusters, fullerenes, and carbonaceous nanoparticles (interstellar grains) (1), an intimate understanding of their formation mechanisms in the interstellar medium (ISM) has been sought from the astrophysics, astrobiology, and astrochemistry communities (2–5). Today, PAH-like molecules are presumed to be ubiquitous in the ISM (6–8), account for 10–30% of the galactic interstellar carbon (9, 10), and provide critical nucleation sites for the formation of carbonaceous dust particles (11, 12). PAHs have also been linked to the unidentified infrared (UIR) emission bands observed in the range of 3–14 μm (3,300–700 cm^{-1}) (13, 14) and to the diffuse interstellar bands (15–17), which are discrete absorption features superimposed on the interstellar extinction curve ranging from the blue part of the visible (400 nm) to the near IR (1.2 μm). The UIR emission features and diffuse interstellar bands are not restricted to our own galaxy as UIR bands have also been observed toward the Cigar Galaxy, M82 (18); a persistent debate has emerged on the role of aliphatic versus aromatic carbon-hydrogen stretches describing the 3.4- μm (2,941- cm^{-1}) feature with methyl-substituted PAHs as potential candidates (19–21). Finally, PAH-like molecules are relevant to the astrobiological evolution of the ISM. In PAHs, the methylidyne (CH) moiety can be replaced by an isoelectronic nitrogen atom, forming biorelevant molecules such as nucleobases—key building blocks in RNA.

Despite the importance of PAH-like molecules in the astrochemical and astrobiological evolution of the ISM, the routes to interstellar PAHs have not been well characterized. The discovery of the simplest PAH, naphthalene (C_{10}H_8), together with more complex PAHs—anthracene/phenanthrene ($\text{C}_{14}\text{H}_{10}$) and pyrene/fluoranthrene ($\text{C}_{16}\text{H}_{10}$), even up to seven-ring ($\text{C}_{28}\text{H}_{16}$) species along with their C1, C2, and C3 alkyl-substituted PAHs—in at least 20 carbonaceous chondrites strongly implies an interstellar origin (22, 23). Sophisticated isotopic studies (e.g., on D, ^{13}C) verified an interstellar source and proposed inner envelopes of carbon-rich asymptotic giant branch (AGB) stars, such as IRC+10216, where temperatures can reach up to a few thousand Kelvin, as the key breeding grounds for these increasingly complex organic molecules (24). Because of the combustion-relevant temperatures of circumstellar envelopes, the most favorable routes to form polycyclic aromatic species have been borrowed from the combustion chemistry community. These pathways have been suggested to involve molecular weight growth processes through sequential reactions of aromatic radicals (ARs) and resonantly stabilized free radicals (RSFRs), such as the phenyl (C_6H_5) and propargyl radicals (C_3H_3), respectively, eventually leading to carbonaceous nanoparticles. Along with acetylene (C_2H_2), these pathways have been contemplated as the basis for the hydrogen abstraction–acetylene addition (HACA) (25–27), phenyl addition–cyclization (28, 29), and ethynyl addition (30) mechanisms. Owing to their stability even at elevated temperatures of several thousand Kelvin, RSFRs and ARs can reach high concentrations in circumstellar environments; these high concentrations make them important reaction intermediates involved in mass growth processes ultimately forming PAHs.

In recent years, based on current models, it has become apparent that PAHs are destroyed faster in the ISM than they can be synthesized (31–33). First, theoretical studies, driven by laboratory studies on the loss of acetylene (C_2H_2) upon the photolysis of small PAHs, predicted lifetimes of a few hundred million years for PAHs in the diffuse ISM. Second, interstellar shock waves driven by supernova explosions forecast similar short lifetimes for PAHs in the ISM (34). Finally, energetic cosmic ray bombardment rapidly degrades small PAHs, once again on a timescale of only a few hundred million years. These timescales are much shorter than the timescale for the injection

of new, PAH-based material into the ISM by carbon-rich AGB stars together with carbon-rich planetary nebulae as the descendants of AGB stars (i.e., around two billion years) (34). Finally, a recent computational study by Mebel and colleagues (35) revealed that the HACA mechanism—the central backbone in contemporary PAH synthesis in circumstellar envelopes of carbon-rich AGB stars—terminates with the formation of naphthalene and acenaphthalene ($C_{12}H_8$). More complex PAHs, even those with only three six-membered rings (anthracene, phenanthrene), cannot be formed via HACA-based pathways. Consequently, the ubiquitous presence of PAHs in the ISM and in carbonaceous chondrites presents a mystery and implies a crucial, hitherto unexplained route to the fast chemical growth of PAHs in the cold environment of the ISM at temperatures as low as 10 K.

To fill the void of rapid and facile formation routes to PAHs, scientists have often looked to ion-molecule reactions as a one-size-fits-all route. The idea of an ion-molecule-dominated interstellar chemistry originated from the 1970s, when the molecular complexity of the ISM was highly underestimated and astrochemists had the misconception that ion-molecule reactions are always barrierless and all neutral-neutral reactions possess entrance barriers. Current astrochemical models speculate that the synthesis of benzene and more complex PAHs is dictated by convoluted networks of ion-molecule reactions involving, for instance, methane (CH_4), ethylene (C_2H_4), and propargyl with $C_2H_3^+$ and $C_4H_2^+$ ions to initially form $C_6H_5^+$ ions (of an unknown structure) (36, 37), which then further react to form PAH-like cations via multistep pathways (38). However, the validity of these routes of PAH formation has remained conjectural, as the outcomes of these bimolecular reactions have often been educationally guessed and not a single laboratory experiment could corroborate the extent to which PAHs are formed in these elementary reactions. Upon the removal of unstudied ion-molecule reactions leading to $C_6H_5^+$, for instance, the peak abundance of $C_6H_5^+$ drops by over three orders of magnitude, resulting in a similar reduction of benzene formed via ion-molecule reactions. Combined with the uncertainties in the assumed rate constant of the association reaction of $C_6H_5^+$ with molecular hydrogen to form $C_6H_7^+$ (39), not even the benzene molecule—the key building block of all PAHs—could be formed in sufficiently high quantities (40). However, the incorporation of barrierless and rapid neutral-neutral reactions involving reactions of ethynyl radicals (C_2H) with 1,3-butadiene (C_4H_6 ; $H_2CCHCHCH_2$) emerged as the most prominent route to synthesize the benzene molecule in cold molecular clouds such as TMC-1, holding temperatures as low as 10 K. These findings also rationalize the detection of benzene with the Infrared Space Observatory toward the protoplanetary nebula CRL 618, with benzene approximately 40 times less abundant than acetylene (41), and suggest the ubiquitous presence of the benzene molecule throughout the ISM. Successive studies of bimolecular neutral-neutral reactions of ethynyl and dicarbon (C_2) with vinylacetylene (C_4H_4), 1,3-butadiene, and isoprene (2-methyl-1,3-butadiene; C_5H_8), exploiting the crossed molecular beam technique and combining reactive scattering data with electronic structure calculations, provided compelling evidence that monocyclic aromatic molecules can be formed via exoergic and fast, barrierless reactions from acyclic precursors as a result of a single collision (**Figure 1**). These investigations delivered the first solid evidence that bimolecular cyclization reactions involving two neutral reactants can synthesize monocyclic aromatic molecules in the gas phase.

This review expands the novel concept of aromatization reactions via bimolecular neutral-neutral collisions from monocyclic systems to PAHs. It compiles the current knowledge on the formation of naphthalene—the simplest PAH—with its derivatives (e.g., hydrogenated naphthalene, mono- and di-methyl-substituted isomers) involving exoergic and fast, barrierless reactions of phenyl-type radicals [e.g., phenyl, *meta*-tolyl (*m*- $C_6H_4CH_3$), *para*-tolyl (*p*- $C_6H_4CH_3$)] with the C4 and C5 hydrocarbons vinylacetylene, 1,3-butadiene, 1-methyl-1,3-butadiene (C_5H_8), and 2-methyl-1,3-butadiene (C_5H_8) as extracted from crossed molecular beam reactions and

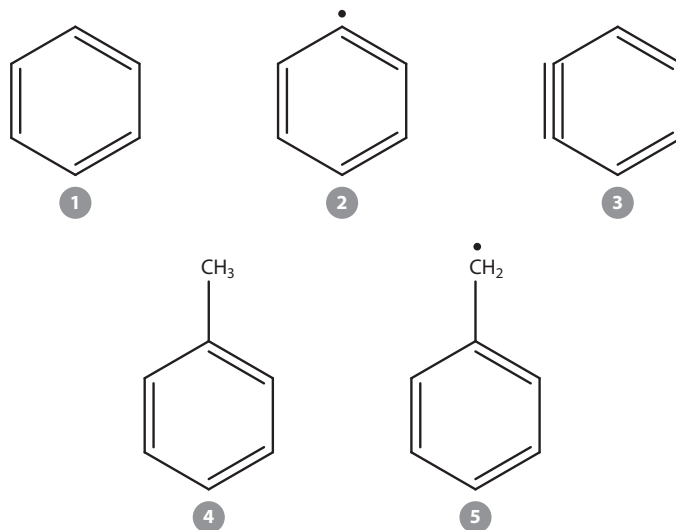


Figure 1

(*Top row*) Monocyclic aromatic molecules formed in exoergic and barrierless bimolecular reactions from ethynyl (C_2H) with 1,3-butadiene (C_4H_6) [benzene; C_6H_6 (1)] (40), dicarbon (C_2) with 1,3-butadiene [phenyl; C_6H_5 (2)] (42), and ethynyl with vinylacetylene (C_4H_4) [*o*-benzyne; C_6H_4 (3)] (43). (*Bottom row*) Substituted monocyclic aromatic molecules formed in exoergic and barrierless bimolecular reactions between ethynyl and 2-methyl-1,3-butadiene (C_5H_8) [toluene; $C_6H_5CH_3$ (4)] (44) and dicarbon with 2-methyl-1,3-butadiene [benzyl; $C_6H_5CH_2$ (5)] (45).

electronic structure calculations. These systems are prototypical representatives of a new class of reactions forming PAHs and their derivatives involving an initial van der Waals complex and a submerged barrier in strongly exoergic processes in the gas phase. These characteristics make bimolecular collisions of phenyl-type radicals with unsaturated C4 and C5 hydrocarbons unique candidates to synthesize (methyl-substituted) PAHs and their partially hydrogenated counterparts in cold molecular clouds at temperatures as low as 10 K, bringing us closer to understanding the formation mechanisms of PAHs in ultracold interstellar environments.

2. THE CROSSED MOLECULAR BEAM APPROACH

Which experimental approach can best reveal the chemical dynamics involved in the formation of PAHs in the gas phase? Experiments conducted under single-collision conditions, in which particles A of one supersonic beam are made to collide only with particles BC of a second beam (Equation 1), are ideal to investigate the chemical dynamics of bimolecular gas phase reactions at the most fundamental, microscopic level (46–58). These are crossed molecular beam experiments. In contrast to bulk experiments, in which reactants are mixed, the crossed beam approach has the unique capability of generating highly reactive radicals, such as phenyl-type radicals ($AR\cdot$) and hydrocarbons (RH) in separate pulsed supersonic beams (Equation 2). In principle, both reactant beams can be prepared in well-defined quantum states before they cross at a specific collision energy under single-collision conditions. These features provide an unprecedented opportunity to observe the consequences of a single-collision event and to identify the nascent reaction products,

excluding secondary collisions and wall effects, ultimately gaining information on the chemical dynamics of the reaction:



Over the past few decades, the use of crossed molecular beams has led to an unprecedented advancement in our understanding of fundamental principles underlying chemical reactivity. Detailed experimental studies of simple three-atom reactions established experimental benchmarks, such as the reactions of chlorine (59, 60), fluorine (61, 62), deuterium (63, 64), carbon (65), nitrogen (58, 66), oxygen (67–69), and sulfur atoms (70) with molecular hydrogen. This approach has been extended to four-atom [OH/CO (71), OH/H₂ (72), CN/H₂ (73)], five-atom [C/C₂H₂ (74)], and six-atom systems [Cl/CH₄ (75), O/CHD₃ (76), F/CD₄ (77)]. These systems are prototypical reactions in bridging our theoretical understanding of reactive scattering via dynamics calculations on chemically accurate potential energy surfaces with experimental observations (78). Although interest in these simple elementary reactions still continues, with the development of powerful theoretical methods, attention has turned in recent years to more complex systems of significant interest in combustion processes and catalysis, as well as interstellar and planetary chemistry (46–58, 79, 80). However, only recently have there been experimental studies of the reactions of phenyl-type radicals with hydrocarbon molecules leading to the formation of PAH-like species under single-collision conditions. This delay resulted from previously insurmountable difficulties of generating stable supersonic beams of phenyl-type radical reactants with sufficiently high concentrations to detect the product molecules.

The formation of PAHs and their hydrogenated as well as methyl-substituted counterparts was explored systematically under single-collision conditions as provided in an ultraclean crossed beam machine (46–50, 52). The main chamber consisted of a stainless steel box evacuated by magnetically suspended turbo molecular pumps to the low 10⁻⁸ Torr region. Two source chambers for separate supersonic beams were located inside the main chamber; in its current geometry, the beams cross perpendicularly. In the primary source, a pulsed supersonic beam of helium-seeded phenyl, *meta*-tolyl, or *para*-tolyl radicals was prepared by photolyzing the appropriate chlorine-substituted precursor molecule [i.e., chlorobenzene (C₆H₅Cl), *meta*-chlorotoluene (*m*-ClC₆H₄CH₃), and *para*-chlorotoluene (*p*-ClC₆H₄CH₃)] at 193 nm. The radical beam passed through a skimmer into the main chamber; a chopper wheel located after the skimmer and prior to the collision center selected slices of the radical beam with well-defined peak velocities tunable between 1,600 and 1,800 ms⁻¹, which then reached the interaction region with typical number densities of approximately $\sim 3 \times 10^{13}$ radicals per cubed centimeter. Each beam was so dilute that collisions within the molecular beam were negligible but were sufficiently dense to monitor the products. This section of the radical beam then intersected a pulsed hydrocarbon beam under well-defined collision energies up to 55 kJ mol⁻¹. Importantly, the incorporation of pulsed supersonic beams is key in untangling the reaction dynamics of PAH formation. First, pulsed UV lasers can be operated in concert with pulsed beams to selectively photolyze the precursor molecule in the molecular beam to form the desired radical reactant. Second, the operation of pulsed valves allows reactions with often-expensive (partially) deuterated chemicals to be carried out; this is crucial to extract key information on the reaction dynamics, such as the position of the hydrogen or deuterium loss(es) if multiple reaction pathways are involved.

Which detection scheme is incorporated for the reaction products? Spectroscopic detection schemes such as laser-induced fluorescence and Rydberg tagging are restricted to hydrogen,

deuterium, and oxygen atoms and to species such as hydroxyl radicals (OH) (i.e., those with well-established spectroscopic fingerprints) (81). Therefore, this approach is not suitable for the detection of PAH-like species, whose a priori spectroscopic properties are, with the exception of naphthalene, unknown. Similarly, it is problematic to identify PAH-type molecules via ion imaging and tunable synchrotron radiation because absolute photoionization cross sections to determine branching ratios do not exist. Therefore, the ultraclean crossed beam machine incorporates a triply differentially pumped, universal quadrupole mass spectrometric detector coupled to an electron impact ionizer operating at extreme ultrahigh vacuum conditions down to the medium 10^{-13} Torr range, which is rotatable within the scattering plane as defined by both beams. Here, any species reactively scattered from the collision center after a single-collision event can be ionized in the electron impact ionizer and in principle can have the mass (and the molecular formula) of all products of a bimolecular reaction determined by varying the mass-to-charge ratio (m/z) in the mass filter. Because of the universal electron impact ionization of the products, even species with unknown spectroscopic properties can be detected. In our setup, we are operating the ionizer at electron energies of 80 eV at an energy at which the ionization cross sections of organic molecules are at their maximum. Our ionizer can also be operated via soft electron impact ionization as pioneered by Casavecchia et al. (57, 58, 80, 82). This approach utilizes electrons with low, tunable energy (8–30 eV) to reduce or even eliminate potential complications from dissociative ionization. However, in the case of the present experiments, soft ionization has one disadvantage: At electron energies of 8–30 eV, the ionization cross sections of the newly formed molecules are at least a factor of 20 lower than the electron impact ionization cross sections with 80-eV electrons (83). Therefore, in the case of pulsed crossed beam experiments with a lower duty cycle compared to continuous sources, soft ionization is impractical. However, soft electron impact ionization was utilized to characterize the primary reactant beams on axis and in situ.

Which observables of key relevance to PAH formation can be extracted from these crossed molecular beam experiments? First, mass spectrometry allows for the determination of the mass and hence the molecular formula of the products of a bimolecular reaction by varying m/z in the mass filter. Second, by systematically exploiting (partially) isotopically labeled reactant molecules, most commonly partially deuterated reactants, one can trace the position of the hydrogen or deuterium loss. For instance, in the reaction of ethynyl radicals with methylacetylene (CH_3CCH), the atomic hydrogen loss leads to the formation of product(s) with a molecular formula C_5H_4 (64 u). However, we cannot determine if the hydrogen atom is lost from the former ethynyl radical, from the methyl group, or from the acetylenic group. Nevertheless, potential atomic hydrogen losses in the crossed beam studies of the $\text{C}_2\text{H-CD}_3\text{CCD}$, $\text{C}_2\text{D-CH}_3\text{CCD}$, and $\text{C}_2\text{D-CD}_3\text{CCH}$ systems enable us to identify the position(s) of the atomic hydrogen loss by tracking the production of ions at the masses corresponding to the isotopologs C_5D_4 , $\text{C}_5\text{H}_2\text{D}_2$, and C_5D_4 at $m/z = 68, 66,$ and 68 , respectively (84–86). Third, because the triply differentially pumped detector is rotatable within the plane defined by both beams, it is possible to map out, at distinct m/z , the laboratory angular distribution and the time of flight spectra of the products from the interaction region over a finite flight distance. By accounting for the apparatus functions as well as angular spreads, a forward-convolution technique transforms the data from the laboratory to the center-of-mass reference frame. These center-of-mass functions [translational energy, $P(E_T)$, and angular distributions, $T(\theta)$] are crucial to untangle the chemical dynamics of the reaction and to identify the nascent reaction products under single-collision conditions. The output of this process is the generation of a product flux contour map, $I(\theta, u) = P(u) \times T(\theta)$, which reports the flux of the reactively scattered products (I) as a function of the center-of-mass scattering angle (θ) and product velocity (u). This function is defined as the reactive differential cross section and can be seen as the image of the chemical reaction containing all the information on the scattering

process. Neither bulk nor kinetic experiments can supply this information. These functions contain some basic information to untangle the underlying chemical dynamics of the reaction.

Considering the center-of-mass translational energy distribution, $P(E_T)$, the maximum translational energy of the products (E_{\max}) can be exploited to obtain the reaction energy. Based on energy conversation, for those products born without internal excitation, subtracting the collision energy from the maximum translational energy of the products yields the exoergicity of the reaction. This is crucially important when different structural isomers with different reaction exoergicities are produced. As discussed above, in the case of polyatomic reactions, it is always useful to conduct the reactions systematically with (partially) deuterated reactants, as multiple structural isomers can be formed. Therefore, by comparing the experimental reaction energies to form (partially) deuterated products at distinct m/z with theoretically computed reaction energies, we can elucidate the product isomers formed together with their branching ratios (87–89). Additionally, in the most favorable case, the distribution maximum of $P(E_T)$ can provide the order of magnitude of the barrier height in the exit channel (87–89). If $P(E_T)$ peaks at zero or close to zero translational energy, the bond rupture within the decomposing reaction intermediate has either no or only a small exit barrier (loose exit transition state). Conversely, $P(E_T)$ can depict pronounced maxima away from zero translational energy, suggesting tight exit transition states and a significant geometry rearrangement, as well as a significant electron density change from the decomposing intermediate to the products resulting in a repulsive bond rupture. The center-of-mass angular distribution [$T(\theta)$] provides information on the reaction mechanism (e.g., direct, indirect, osculating) and might help in estimating the lifetime of the decomposing complex. By comparing the center-of-mass functions with potential energy surfaces and the geometries of reactants, products, and intermediates, one can also infer the reaction intermediate(s) and the nature of the decomposing complex(es). This method can provide direct insight into the nature of the chemical reaction and, in some cases, the preferential rotational axis of the fragmenting complex(es) and the disposal of excess energy into the products' internal degrees of freedom as a function of the scattering angle and collision energy (48). With respect to PAH formation, indirect reactions proceeding via complex formation are critically important. These reactions depict reactive scattering flux over the complete angular range. If the flux contour map portrays a symmetric profile around 90° , the forward-backward symmetry is characteristic of a bimolecular reaction proceeding through a reaction intermediate holding a lifetime longer than its rotation period. The complex lives long enough on the picosecond timescale to rotate several times, and it will have forgotten the directions of the incoming collision partners. The decomposing complex can also have geometrical constraints. For instance, a forward-backward symmetric function, which yields a distribution maximum at 90° , results from a reaction intermediate, which loses a hydrogen atom perpendicularly to the rotational plane of the fragmenting intermediate almost parallel to the total angular momentum vector. Furthermore, the angular flux distribution can be asymmetric around 90° ; often the flux at 0° is larger than that at 180° . In this simple scenario, a so-called osculating complex exists: The reaction is still indirect and proceeds via the formation of an intermediate, but the lifetime of the latter is on the order of the rotation period, and multiple rotations cannot occur. Here, the asymmetry can be used as a clock to estimate the lifetime of the intermediate.

3. RESULTS

3.1. Naphthalene

The formation of naphthalene—the prototypical PAH with two six-membered rings—has been explored via the bimolecular reactions of the phenyl radical with vinylacetylene and the D5-phenyl

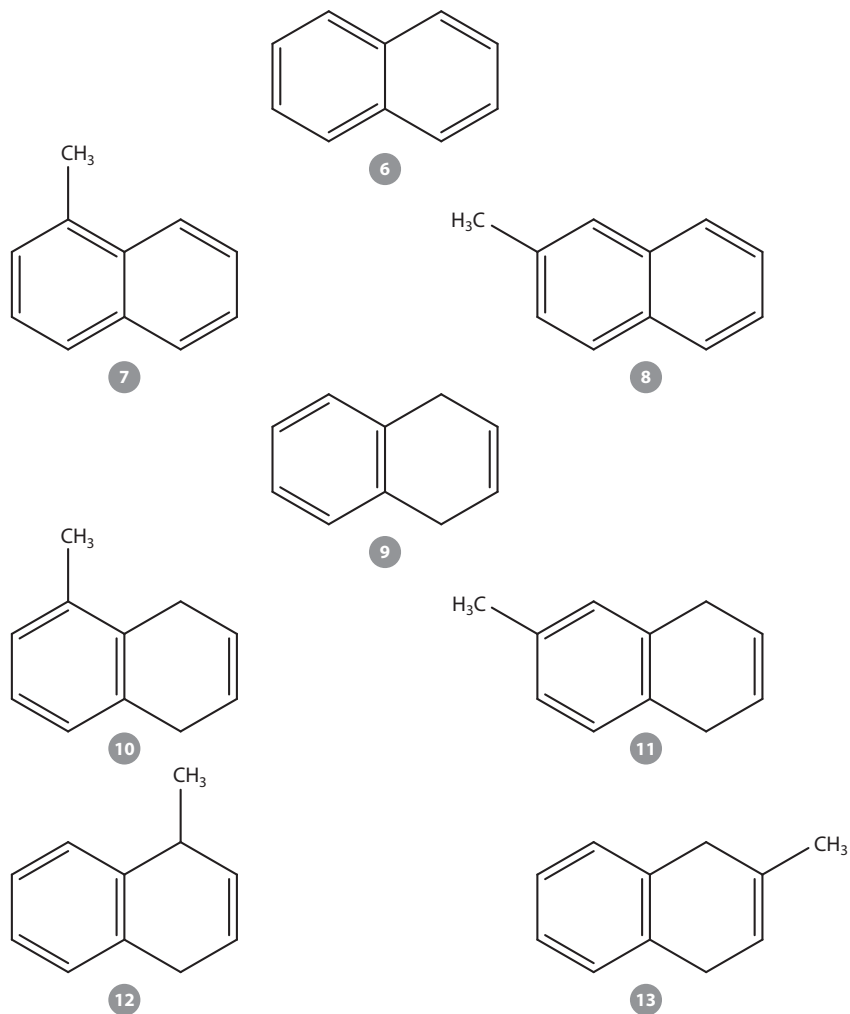


Figure 2

Bicyclic aromatic molecules and their methyl-substituted counterparts formed in exoergic and de facto barrierless bimolecular reactions of phenyl-type radicals with vinylacetylene (C₄H₄), 1,3-butadiene (C₄H₆), and 1-/2-methyl-1,3-butadiene (C₅H₈): (6) naphthalene (C₁₀H₈; phenyl-vinylacetylene), (7) 1-methylnaphthalene (C₁₀H₇CH₃; *meta*-tolyl-vinylacetylene), (8) 2-methylnaphthalene (C₁₀H₇CH₃; *meta/para*-tolyl-vinylacetylene), (9) 1,4-dihydronaphthalene (C₁₀H₁₀; phenyl-1,3-butadiene), (10) 9-methyl-1,4-dihydronaphthalene (C₁₀H₉CH₃; *meta*-tolyl-1,3-butadiene), (11) 8-methyl-1,4-dihydronaphthalene (C₁₀H₉CH₃; *meta/para*-tolyl-1,3-butadiene), (12) 1-methyl-1,4-dihydronaphthalene (C₁₀H₉CH₃; phenyl-1-methyl-1,3-butadiene), and (13) 2-methyl-1,4-dihydronaphthalene (C₁₀H₉CH₃; phenyl-2-methyl-1,3-butadiene) (83, 90–92).

radical (C₆D₅) with vinylacetylene by accessing the C₁₀H₉ potential energy surface (**Figures 2, 3a, and 4a**) (83). For the phenyl-vinylacetylene system, a reactive scattering signal was detected at $m/z = 128$ (C₁₀H₈⁺), indicating that the reaction of the phenyl radical with vinylacetylene leads to the synthesis of a hydrocarbon molecule with the molecular formula C₁₀H₈ plus atomic hydrogen via a single-collision event. The reaction of the D5-phenyl radical with vinylacetylene

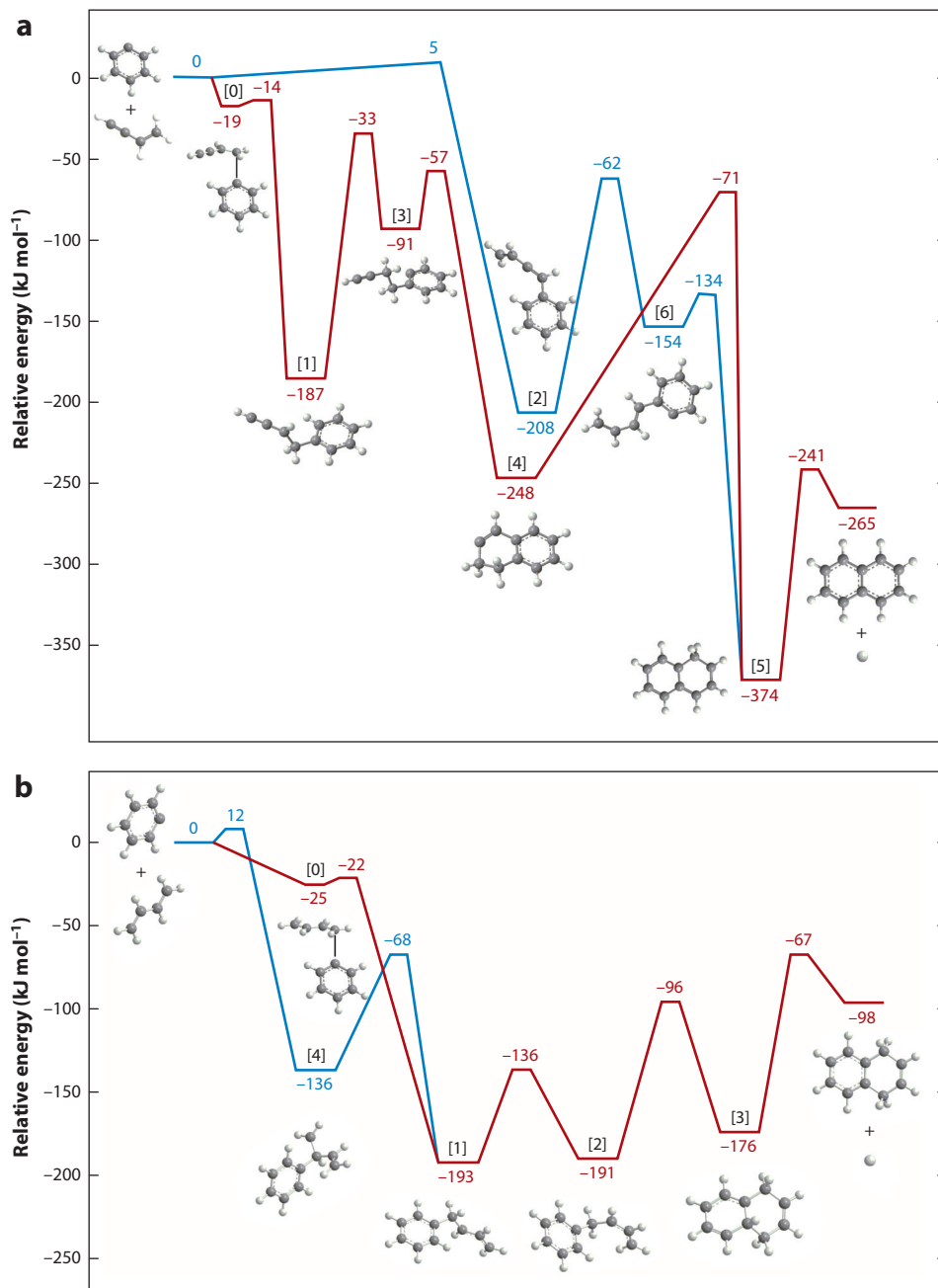


Figure 3

(a) Relevant sections of the potential energy surface of the reaction of phenyl radicals (C_6H_5) with vinylacetylene (C_4H_4) leading to naphthalene in crossed molecular beam reactions (83). The proposed pathway leading to naphthalene in cold molecular clouds is highlighted in red. (b) Relevant sections of the potential energy surface of the reaction of phenyl radicals with 1,3-butadiene (C_4H_6) leading to 1,4-dihydronaphthalene in crossed molecular beam reactions (90). The pathway leading to 1,4-dihydronaphthalene in cold molecular clouds is highlighted in red. Relative energies are given in units of kilojoules per mole.

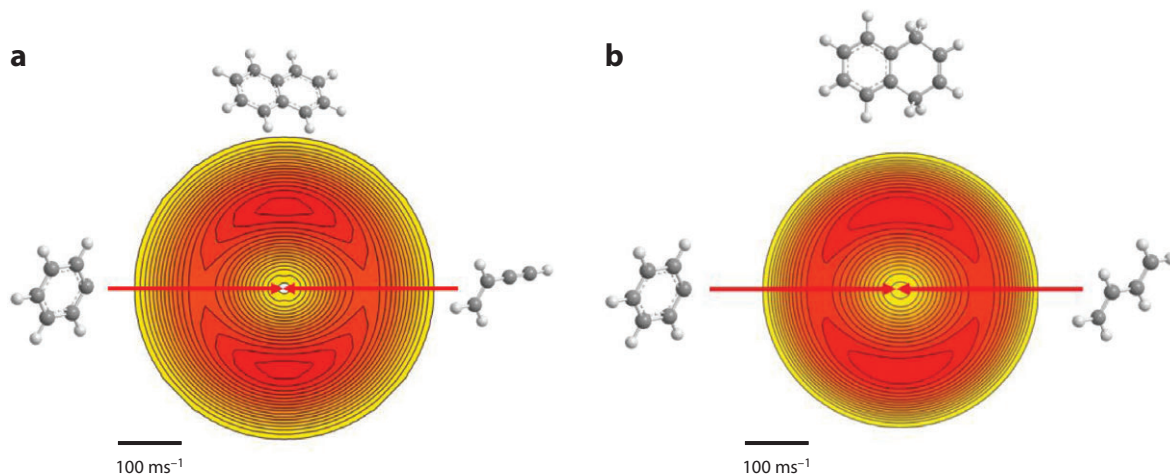


Figure 4

Flux contour plots of the reaction of (a) the phenyl radical with vinylacetylene leading to naphthalene and (b) the phenyl radical with 1,3-butadiene forming 1,4-dihydronaphthalene.

was designed to determine if the hydrogen atom is emitted from the vinylacetylene molecule. A reactive scattering signal was observed at $m/z = 133$ ($C_{10}H_3D_5^+$), indicating that the hydrogen atom is released from the vinylacetylene reactant. Considering that the count rates of the hydrogen atom loss in the reactions of vinylacetylene with phenyl and D5-phenyl radicals are essentially identical within the error limits, the hydrogen atom is suggested to be ejected predominantly from the vinylacetylene reactant and not from the phenyl group. This interpretation of the raw data alone provided convincing evidence that in the reaction of phenyl radicals with vinylacetylene, a hydrocarbon of the molecular formula $C_{10}H_8$ is formed, with atomic hydrogen loss as the driving force and the hydrogen atom originating from the vinylacetylene reactant.

The laboratory data were converted into the center-of-mass frame and combined with electronic structure calculations to identify the product isomer(s) formed (**Figure 3a**). The high-energy cutoffs of the center-of-mass translational energy distributions revealed reaction energies of -268 ± 30 kJ mol $^{-1}$, which are consistent with the formation of at least the naphthalene product. These data agree nicely with the computed data (-265 ± 5 kJ mol $^{-1}$) and data in the literature (-276 ± 18 kJ mol $^{-1}$) to form naphthalene plus atomic hydrogen. We note that the 1-phenyl-vinylacetylene isomer ($C_6H_5HCCHCCH$) is less stable by 223 ± 5 kJ mol $^{-1}$ and cannot account for the experimentally derived reaction energy. Furthermore, the $P(E_T)$ distribution shows a pronounced maximum at 30–40 kJ mol $^{-1}$, indicating the involvement of a tight exit transition state to form naphthalene plus a hydrogen atom. The fact that the center-of-mass angular distribution $T(\theta)$ displays intensity over the complete angular range demonstrates that the reactions follow indirect scattering dynamics through the formation of $C_{10}H_9$ and $C_{10}H_4D_5$ complexes with lifetimes longer than their rotational periods. Most importantly, the $T(\theta)$ distribution has a pronounced maximum at 90°, as is evident from the flux contour plots (**Figure 4a**). This signals sideways scattering and exposes geometrical constraints of the fragmenting $C_{10}H_9/C_{10}H_4D_5$ intermediates, with the hydrogen atom ejected almost parallel to the total angular momentum vector and hence perpendicular to the molecular plane of the rotating, decomposing complex(es).

These findings, combined with electronic structure calculations, and tracing the atomic hydrogen loss with deuterated reactants, allow us to identify two open pathways to naphthalene, among

them one with a de facto barrierless route in the entrance channel. These reactions proceed through addition of the phenyl radical to the terminal C1 and C4 carbon atoms of vinylacetylene to form $C_{10}H_9$ intermediates [1] and [2] shown in **Figure 3a** bound by 187 and 208 kJ mol^{-1} , respectively. Most importantly, when the phenyl radical approaches the C1 carbon atom of vinylacetylene, the potential energy surface is attractive until the formation of a van der Waals complex ([0] in **Figure 3a**), which is weakly stabilized by 19 kJ mol^{-1} with respect to the separated reactants. The further approach leading to the formation of a carbon-carbon bond and intermediate [1] is hindered by a barrier of 5 kJ mol^{-1} , but the corresponding transition state lies lower in energy than the separated phenyl plus vinylacetylene reactants. In this sense, a barrier to addition exists, but this barrier is located below the energy of the separated reactants and is called a submerged barrier. For the overall reaction from phenyl plus vinylacetylene to intermediate [1], the reaction is de facto barrierless. After isomerization to intermediate [1], the latter undergoes a hydrogen shift from the phenyl ring to the vinylacetylene moiety to yield intermediate [3], followed by ring closure to intermediate [4] and a further hydrogen shift, forming intermediate [5]. A hydrogen ejection from the C1 carbon atom of the 1-hydro-naphthalene intermediate (intermediate [5]) leads to naphthalene via a tight exit transition state located 24 kJ mol^{-1} above the products. The competing pathway to naphthalene, via addition to C4, involves an entrance barrier of 5 kJ mol^{-1} . The resulting doublet radical (intermediate [2]) undergoes a hydrogen shift followed by cyclization and naphthalene formation (intermediate [6] \rightarrow intermediate [5] \rightarrow naphthalene plus atomic hydrogen). Our computations also revealed that three monocyclic products—*cis*-1-phenyl-vinylacetylene ($C_6H_5HCCHCCH$), 4-phenyl-vinylacetylene ($C_6H_5CCHCCH_2$), and *trans*-1-phenyl-vinylacetylene ($C_6H_5HCCHCCH$)—are energetically accessible; these isomers, however, are more than 200 kJ mol^{-1} less stable than naphthalene.

At zero pressure and collision energies lower than 5 kJ mol^{-1} , our calculations predict the almost exclusive formation of naphthalene with branching ratios of approximately 99%. Therefore, in cold molecular clouds, where the barrier to addition to C4 cannot be overcome, naphthalene represents the sole reaction product, whose formation is initiated by a van der Waals complex ([0] in **Figure 3a**) and the addition of the phenyl radical to the C1 carbon atom, which holds the vinyl (H_2CCH) moiety, through a submerged barrier, forming intermediate [1]. The successive isomerization sequence intermediate [1] \rightarrow intermediate [3] \rightarrow intermediate [4] \rightarrow intermediate [5] through hydrogen shift \rightarrow cyclization \rightarrow hydrogen shift is terminated by the emission of a hydrogen atom and formation of naphthalene through a tight exit transition state. As predicted experimentally based on the off-zero peaking of the center-of-mass translational energy distribution and also theoretically, the exit transition state is rather tight and located approximately 24 kJ mol^{-1} above the separated products. This can be easily rationalized because the reverse reaction involves the addition of a hydrogen atom to a closed-shell aromatic hydrocarbon, which is associated with an entrance barrier. Finally, the experimentally predicted sideways scattering as visualized in the flux contour plot (**Figure 4a**) is also verified by electronic structure calculations depicting an angle between the plane of the decomposing intermediate and the direction of the atomic hydrogen loss of 81.9° (**Figure 5a**).

3.2. Dihydronaphthalene

The synthesis of 1,4-dihydronaphthalene ($C_{10}H_{10}$)—the prototype of a doubly hydrogenated PAH—was investigated via the bimolecular reactions of the phenyl radical with 1,3-butadiene and D6-1,3-butadiene (C_4D_6) as well as of the D5-phenyl radical with 2,3-D2-1,3-butadiene ($C_4H_4D_2$) and 1,1,4,4-D4-1,3-butadiene ($C_4H_2D_4$) (**Figure 2**) (90). For the phenyl-1,3-butadiene system, a reactive scattering signal probed at $m/z = 130$ ($C_{10}H_{10}^+$) suggested that

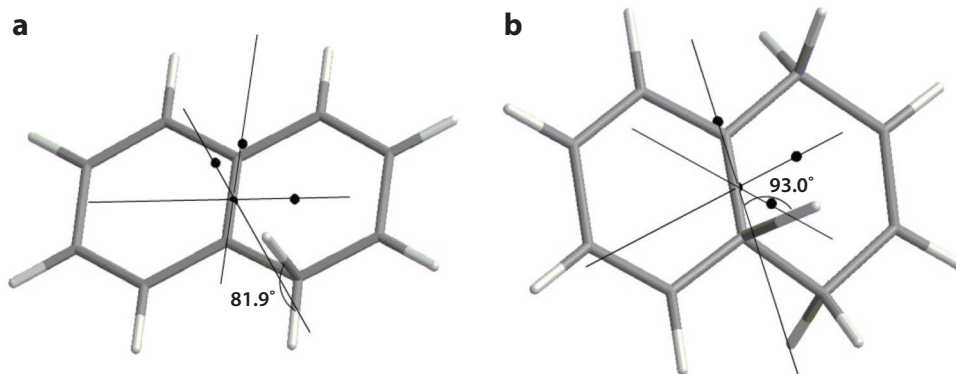


Figure 5

Geometries of the tight exit transition states in the reactions of (a) the phenyl radical with vinylacetylene forming naphthalene and (b) the phenyl radical with 1,3-butadiene forming 1,4-dihydronaphthalene.

the reaction of the phenyl radical with 1,3-butadiene results in the formation of a hydrocarbon with the molecular formula $C_{10}H_{10}$ plus atomic hydrogen via a single-collision event. For the phenyl-D6-1,3-butadiene system, a reactive scattering signal was measured at $m/z = 136$ ($C_{10}D_6H_4^+$); this signal corresponds to hydrogen atom emission from the phenyl ring. The intensity of the hydrogen loss was $58 \pm 15\%$ compared to that in the phenyl-1,3-butadiene system. These findings suggest that the hydrogen atom is emitted from both the phenyl ring and 1,3-butadiene. The hydrogen loss channel in the reaction of partially deuterated 1,3-butadiene molecules with D5-phenyl radicals was monitored to further investigate the extent to which hydrogen emission originated from the 1,3-butadiene molecule. The results of these reactions indicated that the hydrogen emission from the CH_2 group as recorded by tracing the reactive scattering signal at $m/z = 137$ ($C_{10}H_3D_7^+$) in the reaction of 2,3-D2-1,3-butadiene with D5-phenyl accounts for approximately $32 \pm 10\%$ of the signal for the hydrogen loss of the phenyl-1,3-butadiene system, thus accounting for $90 \pm 25\%$ of the hydrogen detected via the partially deuterated reactants compared to the fully hydrogenated system. The interpretation of the raw data alone suggests that in the reaction of phenyl radicals with 1,3-butadiene, a hydrocarbon of the molecular formula $C_{10}H_{10}$ is formed via atomic hydrogen loss; results with (partially) deuterated experiments indicated the formation of at least two structural isomers via hydrogen loss from the phenyl radical and from the CH_2 moiety of the 1,3-butadiene reactant.

The laboratory data were again converted into the center-of-mass frame and combined with electronic structure calculations to ascertain the product isomer(s) formed (**Figure 3b**). The high-energy cutoffs of the center-of-mass translational energy distributions exposed reaction energies of -120 ± 30 kJ mol $^{-1}$, which are consistent with the formation of at least 1,4-dihydronaphthalene. These data agree nicely with the computed data (-98 ± 5 kJ mol $^{-1}$). The *trans*-1-phenyl-1,3-butadiene, *cis*-1-phenyl-1,3-butadiene, and 2-phenyl-1,3-butadiene isomers are less stable by 70–80 kJ mol $^{-1}$ and cannot account for the experimentally derived reaction energies. Moreover, the $P(E_T)$ distribution exhibits a pronounced distribution maximum of 30–40 kJ mol $^{-1}$. These findings suggest the existence of at least one reaction channel that holds a tight exit barrier upon the decomposition of the $C_{10}H_{11}$ intermediate(s). The $T(\theta)$ distribution revealed intensities over the complete angular range, suggesting that the reactions follow indirect scattering dynamics through the formation of $C_{10}H_{11}$ complexes with lifetimes longer than their rotational periods. Furthermore,

the maximum at 90° suggests the existence of geometrical constraints when the reaction intermediate decomposes (i.e., a preferential hydrogen loss parallel to the total angular momentum vector and almost perpendicular to the rotational plane of the decomposing intermediate).

These findings are now being merged with electronic structure calculations (**Figure 3b**). The calculations predict that upon the approach of the phenyl radical to 1,3-butadiene toward the terminal C1 atom, the potential energy surface is attractive until the formation of a van der Waals complex ([0] in **Figure 3b**); this complex is stabilized by 25 kJ mol⁻¹ with respect to the separated reactants. As the carbon-carbon distance continues to decrease, the system proceeds via a submerged barrier located 3 kJ mol⁻¹ above the complex but 22 kJ mol⁻¹ below the reactants. Hence, for the overall reaction from phenyl plus 1,3-butadiene to form intermediate [1], the reaction is de facto barrierless. The intermediate can lose a hydrogen atom from the attacked C1 carbon to form 1-phenyl-*trans*-1,3-butadiene with an overall exoergicity of 36 kJ mol⁻¹ and with the hydrogen atom loss transition state residing 15 kJ mol⁻¹ above 1-phenyl-*trans*-1,3-butadiene plus atomic hydrogen. After the van der Waals complex [0] isomerizes to intermediate [1], the latter undergoes a *trans-cis* isomerization to intermediate [2] followed by ring closure to intermediate [3]. Hydrogen ejection from the bridged carbon atom of intermediate [3] leads to the 1,4-dihydronaphthalene product via a tight exit transition state located 31 kJ mol⁻¹ above the separated products. Additionally, through a barrier of 12 kJ mol⁻¹, the phenyl radical can attack the central carbon atom of 1,3-butadiene, leading to intermediate [4]. Intermediate [4] isomerizes via phenyl group migration to intermediate [1] or ejects a hydrogen atom to the non-PAH isomers. At the low temperature of interstellar clouds of 10 K, only the barrierless addition to C1 forming intermediate [1] is open, whereas the addition to C2 yielding intermediate [4] is closed. Furthermore, the sideways scattering, as verified by a pronounced maximum of the center-of-mass angular distribution at 90° (**Figure 4b**), indicated the existence of geometrical constraints upon decomposition of intermediate [3] (i.e., the emission of the hydrogen atom perpendicular to the rotation plane of the fragmenting intermediate). This has also been authenticated theoretically, and the computations depict an angle of the hydrogen atom loss of 93.0° with respect to the molecular plane (**Figure 5b**). Finally, the product branching ratios computed at zero pressure and collision energies lower than 12 kJ mol⁻¹ reveal that 1,4-dihydronaphthalene clearly dominates the isomer distribution up to approximately 90%.

3.3. (Di)Methyl-Substituted (Dihydro)Naphthalenes

We now transfer the concepts learned from the barrierless formation of two of the simplest representatives of (hydrogenated) PAHs—naphthalene and 1,4-dihydronaphthalene—to methyl- and dimethyl-substituted (dehydrogenated) PAHs, whose structures are compiled in **Figures 2** and **6**, respectively. In the case of naphthalene, a formal replacement of a single hydrogen atom by a methyl group at the C1 and C2 carbon atoms yields 1- and 2-methylnaphthalene (molecules 7 and 8 in **Figure 2**, respectively). Based on the concept of the chemical reactivity of the phenyl radical with vinylacetylene (Section 3.1), we might foresee that a replacement of a hydrogen atom in the phenyl radical reactant by a methyl group should not have any effect on the reaction mechanisms (**Figure 3**). Hence, if the methyl group is replaced at a carbon atom in the phenyl radical far away from the radical center, such as in the *meta* and *para* position, yielding *meta*- and *para*-tolyl, the methyl group should act solely as a spectator without inducing sterical hindrance in the addition process and isomerization via hydrogen migration and ring closure. The results of the crossed molecular beam reactions of vinylacetylene with *meta*-tolyl (92) and *para*-tolyl (91) confirm these predictions. Approaching the C1 atom holding the H₂C moiety of vinylacetylene, both the *meta*- and *para*-tolyl radicals form van der Waals complexes, which are stabilized by

approximately 5 kJ mol^{-1} with respect to the reactants. The complexes lead to the formation of carbon-carbon bonds once again through submerged barriers located only 1 kJ mol^{-1} above the van der Waals complex but 4 kJ mol^{-1} below the energy of the reactants. These pathways lead to the formation of methyl-substituted complexes (intermediate [1] in **Figure 3**), which then undergo isomerization via hydrogen shift \rightarrow cyclization \rightarrow hydrogen shift and hydrogen emission, forming 1- and 2-methylnaphthalenes via tight exit transition states. In cold molecular clouds, the competing additions to C4 have barriers of $\sim 7 \text{ kJ mol}^{-1}$ and hence are closed. In analogy to the reaction of vinylacetylene with the phenyl radical, both the *meta*- and *para*-tolyl radical reactions form methylnaphthalenes with yields of 99% at collision energies of less than 7 kJ mol^{-1} (i.e., lower than the barrier to addition at the C4 carbon atom). It is important to note that because of the molecular structure of the radical reactant, the reaction of the *para*-tolyl radical leads solely to 2-methylnaphthalene, whereas the *meta*-tolyl radical forms 1- and 2-methylnaphthalene upon reaction with vinylacetylene. Here, the hydrogen shift in the methyl-substituted counterpart of intermediate [1] can take place from the C2 and C5 carbon atoms of the phenyl moiety to the C2 atom of the vinylacetylene moiety, resulting in the formation of two chemically nonequivalent methyl-substituted intermediate [3] types, which in turn undergo ring closure to distinct methyl-substituted intermediate [4] types. However, in the case of the *para*-tolyl–vinylacetylene system, both the C2 and C5 positions of the phenyl moiety are chemically equivalent, and only a single methyl-substituted intermediate [3] is formed. In summary, the reaction of *meta*- and *para*-tolyl radicals with vinylacetylene follows the pattern of the barrierless aromatization in the phenyl–vinylacetylene system, leading almost exclusively to 1- and 2-methylnaphthalene under conditions resembling cold molecular clouds.

Having transferred the concept of barrierless ring-closure reactions leading to aromatization from naphthalene to methyl-substituted naphthalenes, we can now shift the principle in a similar pattern from 1,4-dihydronaphthalene to its (di)methyl-substituted counterparts (**Figures 2 and 6**). In the case of 1,4-dihydronaphthalene, the situation is more complex because, compared to naphthalene, both rings are chemically nonequivalent. This can lead to the replacement of a hydrogen atom at the aromatic ring at the C6 and C7 positions, resulting in 9-methyl-1,4-dihydronaphthalene ($\text{C}_{10}\text{H}_9\text{CH}_3$; molecule 10 in **Figure 2**) and 8-methyl-1,4-dihydronaphthalene ($\text{C}_{10}\text{H}_9\text{CH}_3$; molecule 11), or at the olefinic ring, yielding 1-methyl-1,4-dihydronaphthalene ($\text{C}_{10}\text{H}_9\text{CH}_3$; molecule 12) and 2-methyl-1,4-dihydronaphthalene ($\text{C}_{10}\text{H}_9\text{CH}_3$; molecule 13), respectively. Considering that the reaction of the phenyl radical with 1,3-butadiene synthesized the 1,4-dihydronaphthalene molecule (Section 3.2), a hydrogen atom can be replaced in the phenyl ring at the *meta* or *para* positions (i.e., reactions of *meta*- and *para*-tolyl with 1,3-butadiene, forming molecules 10 and 11). Alternatively, a hydrogen atom can be substituted by a methyl group at the C1 and C2 positions of 1,3-butadiene, resulting in reactions of 1-methyl-1,3-butadiene and 2-methyl-1,3-butadiene with phenyl radicals, forming molecules 12 and 13, respectively. All additions to the C1 carbon atom involve the initial formation of a van der Waals complex, which is bound by approximately 7 kJ mol^{-1} with respect to the reactants. After passing a submerged barrier to addition, which is located $4\text{--}5 \text{ kJ mol}^{-1}$ below the energy of the separated reactants, methyl-substituted intermediate [1] is formed, which then undergoes *trans-cis* isomerization, ring closure, and hydrogen loss through tight exit transition states located $29\text{--}40 \text{ kJ mol}^{-1}$ above the products, yielding methyl-substituted 1,4-dihydronaphthalenes (molecules 10–13).

Finally, we explore the reaction mechanisms leading to dimethyl-substituted 1,4-dihydronaphthalenes (**Figure 6**). The replacement of two hydrogen atoms by a methyl group at each ring (aromatic versus olefinic) requires crossed beam experiments in which both reactants hold a methyl group. Both the *meta*- and *para*-tolyl radical reactants fulfill this requirement for the radical reactant, as do the 1- and 2-methyl-1,3-butadiene hydrocarbon reactants. Replacing

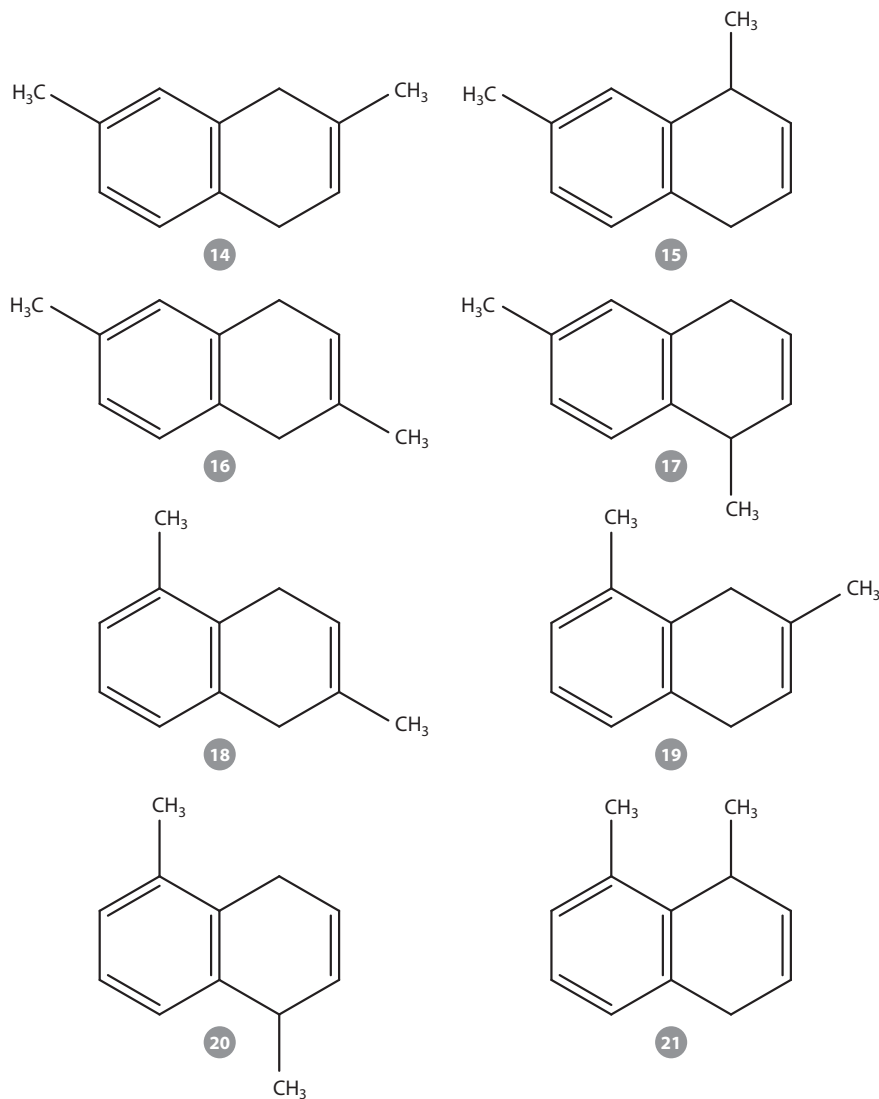


Figure 6

Dimethyl-substituted 1,4-dihydronaphthalene isomers formed in exoergic and de facto barrierless bimolecular reactions of *meta*- and *para*-tolyl radicals with 1-methyl-1,3-butadiene and 2-methyl-1,3-butadiene under single-collision conditions (92).

the hydrogen atoms in the phenyl radical and in the 1,3-butadiene molecule pairwise (**Figure 3**), and tracing the methyl groups in the reaction, leads to the formation of eight distinct dimethyl-substituted 1,4-dihydronaphthalene molecules, as compiled in **Figure 6**. Once again, the addition to the C1 carbon atom of the methyl-substituted 1,3-butadiene reactant is preceded by the formation of a van der Waals complex, which then isomerizes via a submerged barrier to dimethyl-substituted reaction intermediates. Upon *trans-cis* isomerization and cyclization, a terminal hydrogen atom loss through a tight transition state results in the formation of discrete dimethyl-substituted 1,4-dihydronaphthalene isomers.

4. DISCUSSION

Above we demonstrate that de facto barrierless entrance and overall exoergic gas phase reactions of phenyl-type radicals with vinylacetylene and (methyl-substituted) 1,3-butadiene conducted under single-collision conditions lead to the formation of (methyl-substituted) naphthalene and 1,4-dihydronaphthalene. Here we attempt to extract generalized concepts on the chemical reactivity of phenyl-type radicals leading to PAH formation at ultralow temperature conditions in cold molecular clouds of typically 10 K.

All bimolecular reactions of phenyl-type radicals with the C4 and C5 hydrocarbons vinylacetylene and (methyl-substituted) 1,3-butadiene leading to PAH-type products as discussed above are dictated by attractive long-range interaction forces and initiated by the formation of van der Waals complexes, which are weakly bound by 7–25 kJ mol⁻¹ with respect to the separated reactants. PAH formation commences by the addition of the phenyl-type radicals to the C1 carbon atom holding the H₂C moiety of the vinyl group. The barrier to addition is typically 1–5 kJ mol⁻¹ above the van der Waals complex but is below the energy of the separated reactants. Therefore, a barrier to addition does exist, but it is located below the energy of the reactants (submerged barrier), and the reaction proceeds de facto without any entrance barrier. This finding deserves further discussion. Conventional wisdom dictates that the addition of phenyl-type radicals to an olefinic double bond is associated with entrance barriers, for example, 10 kJ mol⁻¹ for ethylene as one of the building blocks of vinylacetylene and 1,3-butadiene. Even though this barrier is quite low, it cannot be overcome at low temperatures of 10 K in cold molecular clouds. However, the enhanced polarizabilities of the C4 and C5 hydrocarbons vinylacetylene and (methyl-substituted) 1,3-butadiene, ranging from 7.7 Å³ to 10.0 Å³, correlate with greater attractive long-range dispersion forces between the phenyl-type radical and the C4/C5 hydrocarbon compared to ethylene (4.15 Å³). The enhanced polarizabilities and attractive long-range dispersion forces trigger the formation of a weakly bound van der Waals complex ([0] in **Figure 3**), which subsequently isomerizes via a submerged barrier. The required existence of a submerged barrier to addition necessitates that the phenyl-type radical must react with a C4 or higher hydrocarbon, which in turn must carry a vinyl group in order to form a weakly bound van der Waals complex. The van der Waals complex subsequently isomerizes via the addition of the phenyl-type radical with its radical center to the H₂C moiety of the vinyl group, forming doublet radicals, which are bound by 180–200 kJ mol⁻¹.

These acyclic doublet radicals undergo multiple rearrangements. In the case of the vinylacetylene reactant, a hydrogen shift from the phenyl-type group to the C2 carbon atom of the vinylacetylene moiety is followed by ring closure and another hydrogen shift, effectively leading to the formation of (methyl-substituted) singly hydrogenated naphthalene intermediates, which then eject a hydrogen atom from C1, forming (methyl-substituted) naphthalenes. The emitted hydrogen atoms originate solely from the H₂C moiety of the vinyl-type group of the vinylacetylene reactant. Considering the (methyl-substituted) 1,3-butadiene reactants, a *trans-cis* isomerization in the addition complex is followed by ring closure, forming (methyl-substituted) singly hydrogenated 1,4-dihydronaphthalene intermediates, which then lose a hydrogen atom from the bridge carbon atom, forming (methyl-substituted) 1,4-dihydronaphthalenes. It is important to highlight that the ejected hydrogen atoms originate solely from the phenyl-type radical and that all exit transition states involving atomic hydrogen loss and aromatization are rather tight and located up to 40 kJ mol⁻¹ above the separated products. Furthermore, in each system, the hydrogen atom is lost almost perpendicularly to the plane of the decomposing complex (**Figures 4 and 5**). This sideways scattering can be rationalized by considering the molecular structures of the naphthalene and 1,4-dihydronaphthalene products. Here, in the reversed reaction, the hydrogen atom has to interact with the π -electron system of the aromatic moieties, which are located perpendicular to

the molecular plane of naphthalene and 1,4-dihydronaphthalene. Finally, at zero pressure and zero collision energy—conditions replicating gas phase conditions of cold molecular clouds—the formation of the PAH-type products is almost quantitative, with typical branching ratios of 99%, with the remaining 1% leading to the formation of non-PAH products, which are thermodynamically less stable typically by 200 and 90 kJ mol⁻¹ for the naphthalene- and 1,4-dihydronaphthalene-type systems, respectively.

We are now testing these generalized concepts of de facto barrierless and exoergic PAH formation via reactions of phenyl-type radicals in an attempt to derive additional prerequisites to PAH formation. First, we tested the prerequisite of a C₄ hydrocarbon reacting with a phenyl-type radical for the reaction to proceed barrierlessly. Our studies of the phenyl-propene (C₃H₆; H₂CCHCH₃) (93) system and of the reactions of phenyl-type radicals (phenyl, *meta*-tolyl, *para*-tolyl) (92, 94) with two C₃H₄ isomers, allene (H₂CCCH₂) and methylacetylene, revealed that these reactions involve barriers to addition of 6–14 kJ mol⁻¹. The absence of van der Waals complexes might be attributed to the lower polarizabilities of the C₃ reactants of only 6.2–6.3 Å³ compared to up to 10.0 Å³ of the C₄ reactants. In the case of the C₃H₄ isomers allene and methylacetylene, both reactions ultimately led to the formation of (methyl-substituted) indene isomers, with indene considered as the prototypical PAH carrying one six- and one five-membered ring (**Figure 7**), however, only after passing an initial entrance barrier to the addition of the phenyl-type radical. Therefore, reactions of phenyl-type radicals with methylacetylene and allene cannot form PAHs

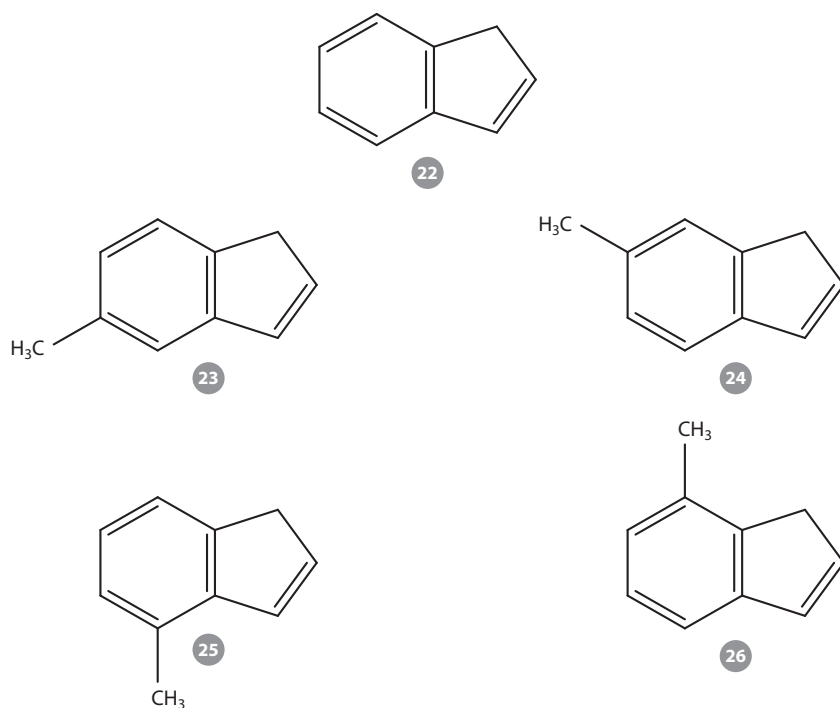


Figure 7

Indene and methyl-substituted indene isomers formed in exoergic reactions involving entrance barriers of phenyl-type radicals (phenyl and *meta*- and *para*-tolyl) with allene and methylacetylene under single-collision conditions (92, 94).

in cold molecular clouds but potentially can in circumstellar envelopes of carbon stars, where elevated temperatures of a few thousand Kelvin help to overcome the barriers to addition. Second, we are investigating the effect of enhanced hydrogen content in the hydrocarbon reactant. With respect to the propene reactant, the propene-phenyl reaction did not lead to the formation of PAH-type products (93, 95). Detailed electronic structure calculations revealed that the initial addition intermediate preferentially decomposed via atomic hydrogen and methyl loss pathways, forming non-PAH products; the synthesis of the PAH derivative indane (C_9H_{10}) would require an addition \rightarrow hydrogen shift \rightarrow cyclization \rightarrow hydrogen loss sequence, in which the transition state for the hydrogen shift is located almost 20 kJ mol^{-1} above the exit barrier to lose a hydrogen atom from the initial collision complex and approximately 9 kJ mol^{-1} above the energy of the separated reactants, thus effectively blocking the formation of indane. The energetically unfavorable nature of this transition state can be readily understood considering that, owing to the enhanced hydrogen content in the hydrocarbon reactant, the resulting doublet radical lacks any resonance stabilization, thus making hydrogen migration energetically less favorable than in the case of indene (C_9H_8) formation. The failed PAH formation in the crossed beam reaction of butene (C_4H_8) with phenyl radicals (95) follows this trend. Conversely, the reaction of phenyl-type radicals with the hydrogen-poor reactants vinylacetylene and 1,3-butadiene involves the formation of RSFR intermediates and, inherently, relatively low-lying atomic hydrogen migration and/or cyclization transition states. However, the enhanced hydrogen content of the butene reactant prohibits the formation of any RSFR intermediate and ultimately PAH formation. Therefore, these considerations suggest that RSFR intermediates and inherently lower barriers to their isomerization reactions, as compared to those for immediate atomic hydrogen loss or carbon-carbon bond cleavage, are crucial to the synthesis of PAH products; enhanced hydrogen content in the reactants inhibits the formation of RSFRs, eventually blocking PAH synthesis.

Finally, we discuss the effect of the molecular structure of the hydrocarbon reactant on PAH formation by comparing the reactivity of four butadiene isomers: 1,3-butadiene, 1-butyne ($HCCC_2H_5$) (89), 2-butyne (CH_3CCCH_3) (89), and 1,2-butadiene [$H_2CCCH(CH_3)$] (96). Combined crossed beam and computational studies revealed that only the reaction of 1,3-butadiene with phenyl (Section 3.2) leads to PAH formation. Reactions of phenyl radicals with the other isomers are dictated by a phenyl radical addition followed by either carbon-carbon or carbon-hydrogen bond rupture processes, leading to non-PAH products. Considering the molecular structures of 1-butyne, 2-butyne, and even 1,2-butadiene, it is evident that the initial addition product has to undergo multiple hydrogen shifts prior to ring closure and hydrogen loss. The lack of formation of resonantly stabilized radical intermediates in these hydrogen migrations again results in energetically unfavorable isomerization steps, which cannot compete with carbon-hydrogen or carbon-carbon bond rupture processes. However, in the case of vinylacetylene ($H_2CCHCCH$) and (methyl-substituted) 1,3-butadiene, resonantly stabilized reaction intermediates can be formed owing to the presence of $-C\equiv CH$ and $-HC=CH_2$ groups in conjugation with the vinyl-type group (H_2CCR ; $R = H, CH_3$), to which the phenyl-type radical is added via a submerged barrier. Therefore, the presence of $-C\equiv CH$ and $-HC=CH_2$ groups in conjugation with a vinyl-type group (H_2CCR ; $R = H, CH_3$), to which the phenyl-type radical is added via a submerged barrier, in a hydrocarbon reactant larger than C_3 is a crucial prerequisite to PAH formation.

5. CONCLUSIONS AND OUTLOOK

Combined crossed beam and electronic structure calculations revealed the facile formation of (methyl-substituted) PAHs, which can be formally derived from naphthalene and 1,4-dihydronaphthalene, upon reaction of phenyl-type radicals with vinylacetylene and

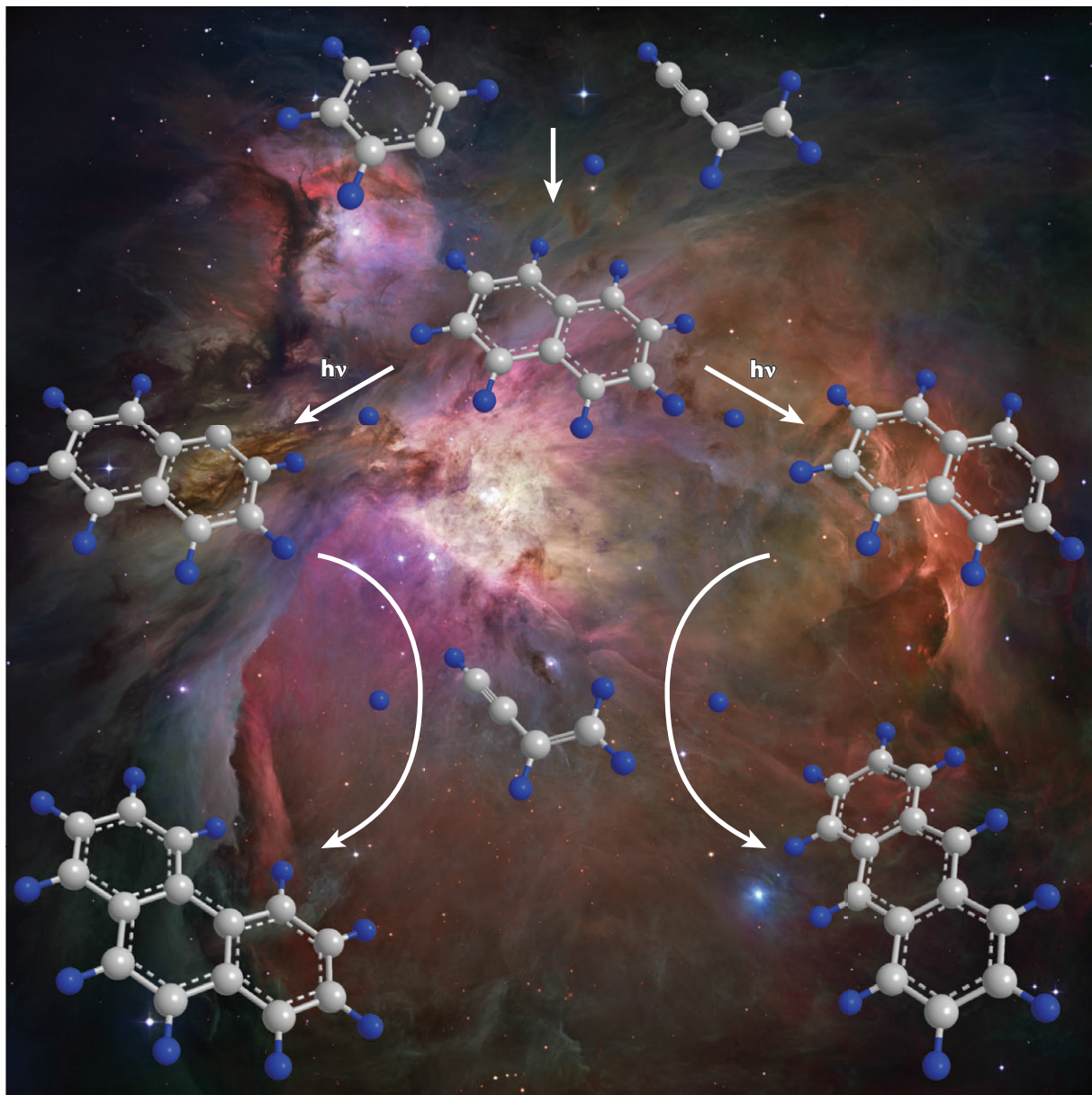


Figure 8

Schematic representation of the stepwise growth of polycyclic aromatic hydrocarbons in the interstellar medium via reactions of phenyl-type radicals with vinylacetylene involving low-temperature chemistry.

(methyl-substituted) 1,3-butadiene. The underlying reaction dynamics involve a de facto barrierless addition of the phenyl-type radical within an initial van der Waals complex through a submerged barrier to a vinyl-type moiety, which must be in conjugation with a $\text{-C}\equiv\text{CH}$ or -HC=CH_2 group in the hydrocarbon reactant to form an RSFR intermediate. These intermediates then rearrange, ultimately forming a cyclic intermediate, which then undergoes aromatization

and PAH formation via atomic hydrogen loss. For the formation of a van der Waals complex, sufficiently strong, attractive, long-range interactions have to be present, suggesting that phenyl-type radicals only form van der Waals complexes with C4 or higher hydrocarbons. In cold molecular clouds, these de facto entrance barrierless, elementary reactions form naphthalene- and 1,4-dihydronaphthalene-based PAHs in yields of up to 99%, also demonstrating the unique connection between RSFR intermediates and PAH formation.

These results are also vital to predict synthetic routes to form more complex PAHs, such as anthracene and phenanthrene, in the ISM, considering that a recent computational study revealed the HACA mechanism to be inefficient in the formation of PAHs beyond acenaphthalene (35). In the ISM, via atomic hydrogen loss from the C1 and C2 positions, the photodissociation of naphthalene can lead to 1- and 2-naphthyl radicals (**Figure 8**) (83). Reactions of the latter with vinylacetylene might propagate PAH extension to systems with three fused benzene rings: anthracene and phenanthrene. These reactions are also expected to be barrierless owing to the much stronger bound van der Waals complex in the entrance channel between vinylacetylene and the naphthyl radical, holding polarizabilities of 7.7 \AA^3 and 16.5 \AA^3 , respectively. Therefore, we might classify the reaction of vinylacetylene with the phenyl radical as the prototype of a class of vinylacetylene-mediated reactions for PAH growth in cold interstellar environments.

To conclude, the simple route to barrierless PAH formation in low-temperature environments via bimolecular reactions involving phenyl-type radicals presents a fundamental shift from previously accepted perceptions of PAH formation via HACA-based pathways and suggests that cold molecular clouds such as TMC-1 and OMC-1 are potential molecular nurseries of PAH synthesis. This view challenges conventional theories that PAHs can be synthesized only in high-temperature environments, such as those present in circumstellar envelopes of evolved carbon stars such as IRC+10216. Therefore, the edges of molecular clouds, at which atomic gas is transformed into molecular gas and carbon drives a complex hydrocarbon chemistry, are likely the prime growth locations of PAH formation via de facto barrierless routes involving two neutral reactants.

DISCLOSURE STATEMENT

The authors are not aware of any affiliations, memberships, funding, or financial holdings that might be perceived as affecting the objectivity of this review.

ACKNOWLEDGMENTS

This work was supported by the US Department of Energy, Basic Energy Sciences, via grants DE-FG02-03ER15411 to R.I.K. at the University of Hawaii and DE-FG02-04ER15570 to A.M.M. at Florida International University.

LITERATURE CITED

1. Puget JL, Leger A. 1989. A new component of the interstellar matter: small grains and large aromatic molecules. *Annu. Rev. Astron. Astrophys.* 27:161–98
2. Cherchneff I. 2011. The formation of polycyclic aromatic hydrocarbons in evolved circumstellar environments. *EAS Publ. Ser.* 46:177–89
3. D’Hendecourt L, Ehrenfreund P. 1997. Spectroscopic properties of polycyclic aromatic hydrocarbons (PAHs) and astrophysical implications. *Adv. Space Res.* 19:1023–32

4. Tielens AGGM, Kerckhoven C, Peeters E, Hony S. 2000. Interstellar and circumstellar PAHs. In *Astrochemistry: From Molecular Clouds to Planetary Systems*, ed. YC Minh, EF van Dishoeck, pp. 349–62. Int. Astron. Union Symp. 197. San Francisco: Astron. Soc. Pac.
5. Ziurys LM. 2006. The chemistry in circumstellar envelopes of evolved stars: following the origin of the elements to the origin of life. *Proc. Natl. Acad. Sci. USA* 103:12274–79
6. Ehrenfreund P, Sephton MA. 2006. Carbon molecules in space: from astrochemistry to astrobiology. *Faraday Discuss.* 133:277–88
7. Rhee YM, Lee TJ, Gudipati MS, Allamandola LJ, Head-Gordon M. 2007. Charged polycyclic aromatic hydrocarbon clusters and the galactic extended red emission. *Proc. Natl. Acad. Sci. USA* 104:5274–78
8. Kim H-S, Wagner DR, Saykally RJ. 2001. Single photon infrared emission spectroscopy of the gas phase pyrene cation: support for a polycyclic aromatic hydrocarbon origin of the unidentified infrared emission bands. *Phys. Rev. Lett.* 86:5691–94
9. Ehrenfreund P, Charnley SB. 2000. Organic molecules in the interstellar medium, comets, and meteorites: a voyage from dark clouds to the early Earth. *Annu. Rev. Astron. Astrophys.* 38:427–83
10. Herbst E, van Dishoeck EF. 2009. Complex organic interstellar molecules. *Annu. Rev. Astron. Astrophys.* 47:427–80
11. Bernstein MP, Sandford SA, Allamandola LJ, Gillette JS, Clemett SJ, Zare RN. 1999. UV irradiation of polycyclic aromatic hydrocarbons in ices: production of alcohols, quinones, and ethers. *Science* 283:1135–38
12. Tielens AGGM. 2008. Interstellar polycyclic aromatic hydrocarbon molecules. *Annu. Rev. Astron. Astrophys.* 46:289–337
13. Ricks AM, Doublerly GE, Duncan MA. 2009. The infrared spectrum of protonated naphthalene and its relevance for the unidentified infrared bands. *Astrophys. J.* 702:301–6
14. Schlemmer S, Cook DJ, Harrison JA, Wurfel B, Chapman W, Saykally RJ. 1994. The unidentified interstellar infrared bands: PAHs as carriers? *Science* 265:1686–89
15. Duley WW. 2006. Polycyclic aromatic hydrocarbons, carbon nanoparticles and the diffuse interstellar bands. *Faraday Discuss.* 133:415–25
16. Ruiterkamp R, Cox NL, Spaans M, Kaper L, Foing BH, et al. 2005. PAH charge state distribution and DIB carriers: implications from the line of sight toward HD 147889. *Astron. Astrophys.* 432:515–29
17. Salama F, Galazutdinov GA, Krelowski J, Allamandola LJ, Musaev FA. 1999. Polycyclic aromatic hydrocarbons and the diffuse interstellar bands: a survey. *Astrophys. J.* 526:265–73
18. Sironi L, Draine BT. 2009. Polarized emission from polycyclic aromatic hydrocarbons resulting from anisotropic illumination. *Astrophys. J.* 698:1292–300
19. Geballe TB, Tielens AGGM, Kwok S, Hrivnak BJ. 1992. Unusual 3 micron emission features in three proto-planetary nebulae. *Astrophys. J.* 387:L89–91
20. Kwok S, Zhang Y. 2011. Mixed aromatic-aliphatic organic nanoparticles as carriers of unidentified infrared emission features. *Nature* 479:80–83
21. Li A, Draine BT. 2012. The carriers of the interstellar unidentified infrared emission features: aromatic or aliphatic? *Astrophys. J.* 760:L31
22. Elsila JE, de Leon NP, Buseck PR, Zare RN. 2005. Alkylation of polycyclic aromatic hydrocarbons in carbonaceous chondrites. *Geochim. Cosmochim. Acta* 69:1349–57
23. Spencer MK, Hammond MR, Zare RN. 2008. Laser mass spectrometric detection of extraterrestrial aromatic molecules: mini-review and examination of pulsed heating effects. *Proc. Natl. Acad. Sci. USA* 105:18096–101
24. Schmitt-Kopplin P, Gabelica Z, Gougeon RD, Fekete A, Kanawati B, et al. 2010. High molecular diversity of extraterrestrial organic matter in Murchison meteorite revealed 40 years after its fall. *Proc. Natl. Acad. Sci. USA* 107:2763–68
25. Frenklach M, Feigelson ED. 1989. Formation of polycyclic aromatic hydrocarbons in circumstellar envelopes. *Astrophys. J.* 341:372–84
26. Frenklach M, Wang H. 1991. Detailed modeling of soot particle nucleation and growth. *Symp. (Int.) Combust.* 23:1559–66

27. Cherchneff I, Barker JR, Tielens AGGM. 1992. Polycyclic aromatic hydrocarbon formation in carbon-rich stellar envelopes. *Astrophys. J.* 401:269–87
28. Shukla B, Koshi M. 2011. Comparative study on the growth mechanisms of PAHs. *Combust. Flame* 158:369–75
29. Shukla B, Tsuchiya K, Koshi M. 2011. Novel products from $C_6H_5 + C_6H_6/C_6H_5$ reactions. *J. Phys. Chem. A* 115:5284–93
30. Mebel AM, Kislov VV, Kaiser RI. 2008. Photoinduced mechanism of formation and growth of polycyclic aromatic hydrocarbons in low-temperature environments via successive ethynyl radical additions. *J. Am. Chem. Soc.* 130:13618–29
31. Micelotta ER, Jones AP, Tielens AGGM. 2011. Polycyclic aromatic hydrocarbon processing by cosmic rays. *Astron. Astrophys.* 526:A52
32. Micelotta ER, Jones AP, Tielens AGGM. 2010. Polycyclic aromatic hydrocarbon processing in a hot gas. *Astron. Astrophys.* 510:A37
33. Micelotta ER, Jones AP, Tielens AGGM. 2010. Polycyclic aromatic hydrocarbon processing in interstellar shocks. *Astron. Astrophys.* 510:A36
34. Kaneda H, Onaka T, Sakon I, Ishihara D, Mouri A, et al. 2011. PAH evolution in the harsh environment of the ISM. *EAS Publ. Ser.* 46:157–68
35. Kislov VV, Sadovnikov AI, Mebel AM. 2013. Formation mechanism of polycyclic aromatic hydrocarbons beyond the second aromatic ring. *J. Phys. Chem. A* 117:4794–816
36. McEwan MJ, Scott GBI, Adams NG, Babcock LM, Terzieva R, Herbst E. 1999. New H and H_2 reactions with small hydrocarbon ions and their roles in benzene synthesis in dense interstellar clouds. *Astrophys. J.* 513:287–93
37. Woods PM, Millar TJ, Zijlstra AA, Herbst E. 2002. The synthesis of benzene in the proto-planetary nebula CRL 618. *Astrophys. J.* 574:L167–70
38. Herbst E. 1991. The in situ formation of large molecules in dense interstellar clouds. *Astrophys. J.* 366:133–40
39. Petrie S, Javahery G, Bohme DK. 1992. Gas-phase reactions of benzenoid hydrocarbon ions with hydrogen atoms and molecules: uncommon constraints to reactivity. *J. Am. Chem. Soc.* 114:9205–6
40. Jones BM, Zhang F, Kaiser RI, Jamal A, Mebel AM, et al. 2011. Formation of benzene in the interstellar medium. *Proc. Natl. Acad. Sci. USA* 108:452–57
41. Cernicharo J, Heras AM, Tielens AGGM, Pardo JR, Herpin F, et al. 2001. Infrared Space Observatory's discovery of C_4H_2 , C_6H_2 , and benzene in CRL 618. *Astrophys. J.* 546:L123–26
42. Zhang F, Jones B, Maksyutenko P, Kaiser RI, Chin C, et al. 2010. Formation of the phenyl radical [$C_6H_5(X^2A_1)$] under single collision conditions: a crossed molecular beam and ab initio study. *J. Am. Chem. Soc.* 132:2672–83
43. Zhang F, Parker DSN, Kim YS, Kaiser RI, Mebel AM. 2011. On the formation of *ortho*-benzyne (*o*- C_6H_4) under single collision conditions and its role in interstellar chemistry. *Astrophys. J.* 728:141
44. Dangi BB, Parker DSN, Kaiser RI, Jamal A, Mebel AM. 2013. A combined experimental and theoretical study on the gas-phase synthesis of toluene under single collision conditions. *Angew. Chem. Int. Ed. Engl.* 52:7186–89
45. Dangi BB, Parker DSN, Yang T, Kaiser RI, Mebel AM. 2014. Gas-phase synthesis of the benzyl radical ($C_6H_5CH_2$). *Angew. Chem. Int. Ed. Engl.* 53:4608–13
46. Gu X, Kaiser RI. 2009. Reaction dynamics of phenyl radicals in extreme environments: a crossed molecular beam study. *Acc. Chem. Res.* 42:290–302
47. Gu X, Guo Y, Zhang F, Mebel AM, Kaiser RI. 2006. Reaction dynamics of carbon-bearing radicals in circumstellar envelopes of carbon stars. *Faraday Discuss.* 133:245–75
48. Kaiser RI. 2002. Experimental investigation on the formation of carbon-bearing molecules in the interstellar medium via neutral-neutral reactions. *Chem. Rev.* 102:1309–58
49. Kaiser RI, Lee TL, Nguyen TL, Mebel AM, Balucani N, et al. 2001. A combined crossed molecular beam and ab initio investigation of C_2 and C_3 elementary reactions with unsaturated hydrocarbons: pathways to hydrogen deficient hydrocarbon radicals in combustion flames. *Faraday Discuss.* 119:51–66

50. Kaiser RI, Maksyutenko P, Ennis C, Zhang F, Gu X, et al. 2010. Untangling the chemical evolution of Titan's atmosphere and surface: from homogeneous to heterogeneous chemistry. *Faraday Discuss.* 147:429–78
51. Kaiser RI, Ochsenfeld C, Stranges D, Head-Gordon M, Lee YT. 1998. Combined crossed molecular beams and ab initio investigation of the formation of carbon-bearing molecules in the interstellar medium via neutral-neutral reactions. *Faraday Discuss.* 109:183–204
52. Kaiser RI, Mebel AM. 2002. The reactivity of ground-state carbon atoms with unsaturated hydrocarbons in combustion flames and in the interstellar medium. *Int. Rev. Phys. Chem.* 21:307–56
53. Balucani N, Zhang F, Kaiser RI. 2010. Elementary reactions of boron atoms with hydrocarbons: toward the formation of organo-boron compounds. *Chem. Rev.* 110:5107–27
54. Parker DSN, Kaiser RI, Mebel AM. 2014. The role of isovalency in the reactions of the cyano (CN), boron monoxide (BO), silicon nitride (SiN), and ethynyl (C₂H) radicals with unsaturated hydrocarbons acetylene (C₂H₂) and ethylene (C₂H₄). *Chem. Soc. Rev.* 43:2701–13
55. Balucani N, Cartechini L, Bergeat A, Casavecchia P, Volpi GG. 2001. Laboratory studies on the formation of CN-containing molecules in the atmosphere of Titan and prebiotic Earth. *EAS Publ. Ser.* 496:159–62
56. Alagia M, Balucani N, Cartechini L, Casavecchia P, Volpi GG. 1997. Dynamics of chemical reactions of astrophysical interest. In *Molecules in Astrophysics: Probes and Processes*, ed. EF van Dishoeck, pp. 271–80. Int. Astron. Union Symp. 178. Dordrecht: Kluwer Acad.
57. Casavecchia P, Balucani N, Volpi GG. 1999. Crossed-beam studies of reaction dynamics. *Annu. Rev. Phys. Chem.* 50:347–76
58. Casavecchia P, Balucani N, Cartechini L, Capozza G, Bergeat A, Volpi GG. 2001. Crossed beam studies of elementary reactions of N and C atoms and CN radicals of importance in combustion. *Faraday Discuss.* 119:27–49
59. Lee S-H, Lai L-H, Liu K, Chang H. 1999. State-specific excitation function for Cl(²P)+H₂ (*v* = 0, *j*): effects of spin-orbit and rotational states. *J. Chem. Phys.* 110:8229–32
60. Alagia M, Balucani N, Cartechini L, Casavecchia P, van Kleef EH, et al. 1996. Dynamics of the simplest chlorine atom reaction. *Science* 273:1519–22
61. Neumark DM, Wodtke AM, Robinson GN, Hayden CC, Lee YT. 1984. Experimental investigation of resonances in reactive scattering: the atomic fluorine + molecular hydrogen reaction. *Phys. Rev. Lett.* 53:226–29
62. Neumark DM, Wodtke AM, Robinson GN, Hayden CC, Shobatake K, et al. 1985. Molecular beam studies of F + D₂ and F + HD reactions. *J. Chem. Phys.* 82:3067–77
63. Continetti RE, Balko BA, Lee YT. 1990. Crossed molecular beams study of the reaction D + H₂ → DH + H at collision energies of 0.53 and 1.01 eV. *J. Chem. Phys.* 93:5719–40
64. Kitsopoulos TN, Buntine MA, Baldwin DP, Zare RN, Chandler DW. 1993. Reaction product imaging: the H + D₂ reaction. *Science* 260:1605–10
65. Guadagnini R, Schatz GC. 1996. Unusual insertion mechanism in the reaction C(³P) + H₂ → CH + H. *J. Phys. Chem.* 100:18944–49
66. Alagia M, Balucani N, Cartechini L, Casavecchia P, Volpi GG, et al. 1999. Exploring the reaction dynamics of nitrogen atoms: a combined crossed beam and theoretical study of N(²D) + D₂ → ND + D. *J. Chem. Phys.* 110:8857–60
67. Hsu Y-T, Liu K, Pederson LA, Schatz GC. 1999. Reaction dynamics of O(¹D) + HD. II. Effects of excited surfaces. *J. Chem. Phys.* 111:7931–44
68. Hsu Y-T, Liu K, Pederson LA, Schatz GC. 1999. Reaction dynamics of O(¹D) + HD. I. The insertion pathway. *J. Chem. Phys.* 111:7921–30
69. Che D-C, Liu K. 1995. Reactive scattering of O(¹D) + HD: product speed and angle distributions. *J. Chem. Phys.* 103:5164–67
70. Chao SD, Skodje RT. 2001. Quasi-classical trajectory studies of the insertion reactions S(¹D) + H₂, HD, and D₂. *J. Phys. Chem. A* 105:2474–84
71. Alagia M, Balucani N, Casavecchia P, Stranges D, Volpi GG. 1993. Crossed beam studies of four atom reactions: the dynamics of OH + CO. *J. Chem. Phys.* 98:8341–44

72. Strazisar BR, Lin C, Davis HF. 2000. Mode-specific energy disposal in the four-atom reaction $\text{OH} + \text{D}_2 \rightarrow \text{HOD} + \text{D}$. *Science* 290:958–61
73. Takayanagi T, Schatz GC. 1997. Reaction dynamics calculations for the $\text{CN} + \text{H}_2 \rightarrow \text{HCN} + \text{H}$ reaction: applications of the rotating-bond approximation. *J. Chem. Phys.* 106:3227–36
74. Park WK, Park J, Park SC, Braams BJ, Chen C, Bowman JM. 2006. Quasiclassical trajectory calculations of the reaction $\text{C} + \text{C}_2\text{H}_2 \rightarrow \text{I-C}_3\text{H}$, $\text{c-C}_3\text{H} + \text{H}$, $\text{C}_3 + \text{H}_2$ using full-dimensional triplet and singlet potential energy surfaces. *J. Chem. Phys.* 125:081101
75. Zhang B, Liu K, Czako G, Bowman JM. 2012. Translational energy dependence of the $\text{Cl} + \text{CH}_4(v_b = 0, 1)$ reactions: a joint crossed-beam and quasiclassical trajectory study. *Mol. Phys.* 110:1617–26
76. Czako G, Bowman JM. 2012. Dynamics of the $\text{O}(^3\text{P}) + \text{CHD}_3(v_{\text{CH}} = 0, 1)$ reactions on an accurate ab initio potential energy surface. *Proc. Natl. Acad. Sci. USA* 109:7997–8001
77. Wang F, Liu K. 2011. Experimental signatures for a resonance-mediated reaction of bend-excited $\text{CD}_4(v_b = 1)$ with fluorine atoms. *Phys. Chem. Lett.* 2:1421–25
78. Bowman JM, Czako G, Fu B. 2011. High-dimensional ab initio potential energy surfaces for reaction dynamics calculations. *Phys. Chem. Chem. Phys.* 13:8094–111
79. Albert DR, Davis HF. 2013. Studies of bimolecular reaction dynamics using pulsed high-intensity vacuum-ultraviolet lasers for photoionization detection. *Phys. Chem. Chem. Phys.* 15:14566–80
80. Casavecchia P, Leonori F, Balucani N, Petrucci R, Capozza G, Segoloni E. 2009. Probing the dynamics of polyatomic multichannel elementary reactions by crossed molecular beam experiments with soft electron-ionization mass spectrometric detection. *Phys. Chem. Chem. Phys.* 11:46–65
81. Liu K. 2001. Crossed-beam studies of neutral reactions: state-specific differential cross sections. *Annu. Rev. Phys. Chem.* 52:139–64
82. Capozza G, Segoloni E, Leonori F, Volpi GG, Casavecchia P. 2004. Soft electron impact ionization in crossed molecular beam reactive scattering: the dynamics of the $\text{O}(^3\text{P}) + \text{C}_2\text{H}_2$ reaction. *J. Chem. Phys.* 120:4557–60
83. Parker DSN, Zhang F, Kim YS, Kaiser RI, Landera A, et al. 2012. Low temperature formation of naphthalene and its role in the synthesis of PAHs (polycyclic aromatic hydrocarbons) in the interstellar medium. *Proc. Natl. Acad. Sci. USA* 109:53–58
84. Kaiser RI, Chiong CC, Asvany O, Lee YT, Stahl F, et al. 2001. Chemical dynamics of d1-methyldiacetylene (CH_3CCCCD ; X^1A_1) and d1-ethynylallene ($\text{H}_2\text{CCCH}(\text{C}_2\text{D})$; X^1A') formation from reaction of $\text{C}_2\text{D}(X^2\Sigma^+)$ with methylacetylene $\text{CH}_3\text{CCH}(X^1A_1)$. *J. Chem. Phys.* 114:3488–96
85. Stahl F, von Ragué Schleyer P, Bettinger HF, Kaiser RI, Lee YT, Schaefer HF III. 2001. Reaction of the ethynyl radical, C_2H , with methylacetylene, CH_3CCH , under single collision conditions: implications for astrochemistry. *J. Chem. Phys.* 114:3476–87
86. Stahl F, von Ragué Schleyer P, Schaefer HF III, Kaiser RI. 2002. Reactions of ethynyl radicals as a source of C_4 and C_5 hydrocarbons in Titan's atmosphere. *Planet. Space Sci.* 50:685–92
87. Gu X, Zhang F, Guo Y, Kaiser RI. 2007. Reaction dynamics of phenyl radicals (C_6H_5) with methylacetylene (CH_3CCH), allene (H_2CCCH_2), and their D4-isotopomers. *J. Phys. Chem. A* 111:11450–59
88. Zhang F, Maksyutenko P, Kaiser RI. 2012. Chemical dynamics of the $\text{CH} + \text{C}_2\text{H}_4$, $\text{CH} + \text{C}_2\text{D}_4$, and $\text{CD} + \text{C}_2\text{H}_4$ reactions studied under single collision conditions. *Phys. Chem. Chem. Phys.* 14:529–37
89. Kaiser RI, Gu X, Zhang F, Maksyutenko P. 2012. Crossed beam reaction of methylidyne [$\text{CH}(X^2\Pi)$] with D₂-acetylene [$\text{C}_2\text{D}_2(X^1\Sigma_g^+)$] and D1-methylidyne [$\text{CD}(X^2\Pi)$] with acetylene [$\text{C}_2\text{H}_2(X^1\Sigma_g^+)$]. *Phys. Chem. Chem. Phys.* 14:575–88
90. Kaiser RI, Parker DSN, Zhang F, Landera A, Kislov VV, Mebel AM. 2012. PAH formation under single collision conditions: reaction of phenyl radical and 1,3-butadiene to form 1,4-dihydronaphthalene. *J. Phys. Chem. A* 116:4248–58
91. Parker DSN, Dang BB, Kaiser RI, Jamal A, Ryazantsev MN, et al. 2014. An experimental and theoretical study on the formation of 2-methylnaphthalene ($\text{C}_{11}\text{H}_{10}/\text{C}_{11}\text{H}_3\text{D}_7$) in the reactions of the para-tolyl (C_7H_7) and para-tolyl-d7 (C_7D_7) with vinylacetylene (C_4H_4). *J. Phys. Chem. A* 118:2709–18
92. Parker DSN, Yang T, Kaiser RI. 2014. Submitted manuscript
93. Kaiser RI, Parker DSN, Goswami M, Zhang F, Kislov VV, et al. 2012. Crossed beam reaction of phenyl and D5-phenyl radicals with propene and deuterated counterparts: competing atomic hydrogen and methyl loss pathways. *Phys. Chem. Chem. Phys.* 14:720–29

94. Parker DSN, Zhang F, Kaiser RI, Kislov VV, Mebel AM. 2011. Indene formation under single-collision conditions from the reaction of phenyl radicals with allene and methylacetylene: a crossed molecular beam and ab initio study. *Chem. Asian J.* 6:3035–47
95. Albert DR, Todt MA, Davis HF. 2013. Crossed molecular beams studies of phenyl radical reactions with propene and *trans*-2-butene. *J. Phys. Chem. A* 117:13967–75
96. Yang T, Parker DSN, Dangi BB, Kaiser RI, Kislov VV, Mebel AM. 2014. Crossed beam reactions of the phenyl (C_6H_5 ; X^2A_1) and phenyl-d5 radical (C_6D_5 ; X^2A_1) with 1,2-butadiene ($H_2CCCHCH_3$; X^1A'). *J. Phys. Chem. A* 118:6181–90



Contents

Molecules in Motion: Chemical Reaction and Allied Dynamics in Solution and Elsewhere <i>James T. Hynes</i>	1
Crystal Structure and Prediction <i>Tejender S. Thakur, Ritesh Dubey, and Gautam R. Desiraju</i>	21
Reaction Dynamics in Astrochemistry: Low-Temperature Pathways to Polycyclic Aromatic Hydrocarbons in the Interstellar Medium <i>Ralf I. Kaiser, Dorian S.N. Parker, and Alexander M. Mebel</i>	43
Coherence in Energy Transfer and Photosynthesis <i>Aurélia Chenu and Gregory D. Scholes</i>	69
Ultrafast Dynamics of Electrons in Ammonia <i>Peter Vöhringer</i>	97
Dynamics of Bimolecular Reactions in Solution <i>Andrew J. Orr-Ewing</i>	119
The Statistical Mechanics of Dynamic Pathways to Self-Assembly <i>Stephen Whitelam and Robert L. Jack</i>	143
Reaction Dynamics at Liquid Interfaces <i>Ilan Benjamin</i>	165
Quantitative Sum-Frequency Generation Vibrational Spectroscopy of Molecular Surfaces and Interfaces: Lineshape, Polarization, and Orientation <i>Hong-Fei Wang, Luis Velarde, Wei Gan, and Li Fu</i>	189
Mechanisms of Virus Assembly <i>Jason D. Perlmutter and Michael F. Hagan</i>	217
Cold and Controlled Molecular Beams: Production and Applications <i>Justin Jankunas and Andreas Osterwalder</i>	241
Spintronics and Chirality: Spin Selectivity in Electron Transport Through Chiral Molecules <i>Ron Naaman and David H. Waldeck</i>	263

DFT: A Theory Full of Holes? <i>Aurora Pribram-Jones, David A. Gross, and Kieron Burke</i>	283
Theoretical Description of Structural and Electronic Properties of Organic Photovoltaic Materials <i>Andriy Zhubayevych and Sergei Tretiak</i>	305
Advanced Physical Chemistry of Carbon Nanotubes <i>Jun Li and Gai P. Pandey</i>	331
Site-Specific Infrared Probes of Proteins <i>Jianqiang Ma, Ileana M. Pazos, Wenkai Zhang, Robert M. Culik, and Feng Gai</i>	357
Biomolecular Damage Induced by Ionizing Radiation: The Direct and Indirect Effects of Low-Energy Electrons on DNA <i>Elabe Alizadeh, Thomas M. Orlando, and Léon Sanche</i>	379
The Dynamics of Molecular Interactions and Chemical Reactions at Metal Surfaces: Testing the Foundations of Theory <i>Kai Golibrzuch, Nils Bartels, Daniel J. Auerbach, and Alec M. Wodtke</i>	399
Molecular Force Spectroscopy on Cells <i>Baoyu Liu, Wei Chen, and Cheng Zhu</i>	427
Mass Spectrometry of Protein Complexes: From Origins to Applications <i>Shahid Mehmood, Timothy M. Allison, and Carol V. Robinson</i>	453
Low-Temperature Kinetics and Dynamics with Coulomb Crystals <i>Brianna R. Heazlewood and Timothy P. Softley</i>	475
Early Events of DNA Photodamage <i>Wolfgang J. Schreier, Peter Gilch, and Wolfgang Zinth</i>	497
Physical Chemistry of Nanomedicine: Understanding the Complex Behaviors of Nanoparticles in Vivo <i>Lucas A. Lane, Ximei Qian, Andrew M. Smith, and Shuming Nie</i>	521
Time-Domain Ab Initio Modeling of Photoinduced Dynamics at Nanoscale Interfaces <i>Linjun Wang, Run Long, and Oleg V. Prezhdo</i>	549
Toward Design Rules of Directional Janus Colloidal Assembly <i>Jie Zhang, Erik Luijten, and Steve Granick</i>	581
Charge Transfer-Mediated Singlet Fission <i>N. Monahan and X.-Y. Zhu</i>	601
Upconversion of Rare Earth Nanomaterials <i>Ling-Dong Sun, Hao Dong, Pei-Zhi Zhang, and Chun-Hua Yan</i>	619

Computational Studies of Protein Aggregation: Methods and Applications <i>Alex Morriss-Andrews and Joan-Emma Shea</i>	643
Experimental Implementations of Two-Dimensional Fourier Transform Electronic Spectroscopy <i>Franklin D. Fuller and Jennifer P. Ogilvie</i>	667
Electron Transfer Mechanisms of DNA Repair by Photolyase <i>Dongping Zhong</i>	691
Vibrational Energy Transport in Molecules Studied by Relaxation-Assisted Two-Dimensional Infrared Spectroscopy <i>Natalia I. Rubtsova and Igor V. Rubtsov</i>	717

Indexes

Cumulative Index of Contributing Authors, Volumes 62–66	739
Cumulative Index of Article Titles, Volumes 62–66	743

Errata

An online log of corrections to *Annual Review of Physical Chemistry* articles may be found at <http://www.annualreviews.org/errata/physchem>